THE EFFECTS OF PLATINUM PARTICLE SIZE TO THE EFFICIENCY OF A DYE SENSITIZED SOLAR CELL (DSSC)

A THESIS SUBMITTED TO
THE GRADUATE SCHOOL OF NATURAL AND APPLIED SCIENCES
OF
MIDDLE EAST TECHNICAL UNIVERSITY

BY

HASAN BERK GİRAY

IN PARTIAL FULFILLMENT OF THE REQUIREMENTS
FOR
THE DEGREE OF MASTER OF SCIENCE
IN
CHEMICAL ENGINEERING

JANUARY 2010

Approval of the thesis:

THE EFFECTS OF THE PLATINUM PARTICLE SIZE TO THE EFFICIENCY OF A DYE SENSITIZED SOLAR CELL (DSSC)

submitted by **HASAN BERK GİRAY** in partial fulfillment of the requirements for the degree of **Master of Science in Chemical Engineering Department, Middle East Technical University** by,

Prof. Dr. Canan Özgen _____
Dean, Graduate School of **Natural and Applied Sciences**

Prof. Dr. Gürkan Karakaş _____
Head of Department, **Chemical Engineering**

Prof. Dr. Deniz Üner _____
Supervisor, **Chemical Engineering Dept., METU**

Prof. Dr. Engin Umut Akkaya _____
Co-Supervisor, **Chemistry Dept., Bilkent University**

Examining Committee Members:

Prof. Dr. Gürkan Karakaş _____
Chemical Engineering Dept., METU

Prof. Dr. Deniz Üner _____
Chemical Engineering Dept., METU

Prof. Dr. Hayrettin Yücel _____
Chemical Engineering Dept., METU

Prof. Dr. Raşit Turan _____
Physics Dept., METU

Assist. Prof. Barış Bayram _____
Electrical and Electronics Engineering Dept., METU

Date _____

I hereby declare that all information in this document has been obtained and presented in accordance with academic rules and ethical conduct. I also declare that, as required by these rules and conduct, I have fully cited and referenced all material and results that are not original to this work.

Name, Last Name: Hasan Berk GİRAY

Signature :

ABSTRACT

THE EFFECTS OF THE PLATINUM PARTICLE SIZE TO THE EFFICIENCY OF A DYE SENSITIZED SOLAR CELL (DSSC)

Giray, Hasan Berk

M.S., Department of Chemical Engineering

Supervisor: Prof. Dr. Deniz Üner

Co-Supervisor: Prof. Dr. Engin Umut Akaya

January 2010, 69 pages

The aim of this study was to modify the platinum particle size to observe the effects on the efficiency of a Dye Sensitized Solar Cell (DSCC). DSSC was prepared as follows: On the anode side, TiO_2 was annealed on the transparent conducting oxide (TCO) which is SnO_2:F coated and a cis-bis (isothiocyanato) bis (2,2'-bipyridyl-4,4'-dicarboxylato)–ruthenium(II) dye was adsorbed on the TiO_2. On the cathode side, platinum was coated on TCO from an alcohol based solution of platinum (plasitol) by thermal decomposition method. Potassium iodide and iodine were dissolved in ethylene glycol to prepare the electrolyte.

Four cathode surfaces were prepared by thermal decomposition method at 400 ^{o}C and 5 min. Cathode surface morphology was changed by changing the annealing conditions. Current-voltage measurements were performed for determining the cell efficiency. One cathode glass was used as such giving a cell efficiency of 2.36%. Three glasses were further thermally treated at 450 ^{o}C, 500 ^{o}C and 550 ^{o}C for 30 min. highest efficiency was measured with the counter electrode annealed at 550 ^{o}C for 30 min as 2.89%.

SEM micrographs of the substrate which was SnO_2:F coated TCO revealed a decrease in average surface particle size with an increase in annealing temperature. EDX mappings showed that as the annealing temperature increased, Pt particles segregated together to form porous patches.

In this study, it was demonstrated that as the annealing temperature of cathode increased, DSSC efficiency increased. These results can be used to design cheaper DSSCs with higher efficiencies.

Keywords: DSSC, solar cell, solar panel, platinum

ÖZ

PLATİN PARÇACIK BOYUTUNUN DUYARLILAŞTIRILMIŞ BOYA GÜNEŞ PANELİ (DBGP) VERİMLİLİĞİNE ETKİSİ

Giray, Hasan Berk
Yüksek Lisans, Kimya Mühendisliği Bölümü
Tez Yöneticisi: Prof. Dr. Deniz Üner
Ortak Tez Yöneticisi: Prof. Dr. Engin Umut Akkaya

Ocak 2010, 69 sayfa

Bu çalışmanın amacı, platin parçacık boyutlarının Duyarlılaştırılmış Boya Güneş Pili (DBGP) verimliliği üzerindeki etkisinin incelenmesidir. Anodun hazırlanması için, TiO_2, SnO_2:F kaplamalı geçirgen iletken oksit (GİO) üzerine tav edildi ve sonrasında cis-bis (isothiocyanato)bis(2,2'-bipyridyl-4,4'-dicarboxylato) - ruthenium (II) boya, tav edilmiş olan TiO_2 üzerine adsorblandı. Platinin alkol bazlı bir karışımının (plasitol) GİO üzerine ısıl parçalanma yolu kullanılarak kaplanması ile DBGP'nin katodu hazırlandı. Potasyum iyodür ve iyotun, etilen glikol içinde çözülmesi ile elektrolit çözelti hazırlandı.

Dört değişik katot yüzey, Plasitol'ün GİO yüzeyine fırça ile uygulanması ve ısıl parçalanma için 400 ^{o}C sıcaklıkta 5 dakika tutulması ile hazırlandı. Tav edilme koşullarının değiştirilmesi ile katod yüzey morfolojisi değiştirildi. Akım-voltaj ölçümleri verimlilik hesaplamaları için gerçekleştirildi. Bu yüzeylerin birisi kullanılarak DBGP verimi 2.36% olarak ölçüldü. Diğer üç camın her biri, 450 ^{o}C, 500 ^{o}C e 550 ^{o}C 30 dakika tavlanarak farklı yüzey mofolojileri elde edildi. En yüksek verim 550 ^{o}C sıcaklıkta tav edilmiş katot ile 2.89% olarak elde edildi.

SnO_2:F kaplı cam alttaş'ın SEM resimleri, tavlanma sıcaklığı ile yüzey ortalama parçacık boyutunun azaldığını gösterildi. Tavlanma sıcaklığının artması ile Pt parçacıklarının gözenekli ağyapılar oluşturdukları EDX haritalandırması ile gözlemlendi.

Bu çalışmada, yüksek tavlama sıcaklığı ile hazırlanan katotların DBGP verimliliğini yükselttiği gösterilmiştir. Bu sonuç, platinin daha verimli kullanıldığı DBGP üretimi için kullanılabilir.

Anahtar kelimeler: DBGP, güneş hücresi, güneş paneli, platin

to my sunshine

ACKNOWLEDGMENTS

I would like to thank to my supervisor Prof. Dr. Deniz Üner for her guidance, encouragements, positive criticism and support throughout this study. Her wisdom both about this study and my life is always be unforgettable. I am also thankful to my co-supervisor Prof. Dr. Engin Umut Akkaya for his cooperation. I am grateful to Prof. Dr. Gürkan Karakaş for allowing to use his facilities.

I am also thankful to my wife, Esra Giray. She is the sun shine to both my life and my thesis study. Everything is meaningful with her.

I am also deeply thankful to my mother Tuna Giray, my father Haldun Giray, my brother Tolga Giray and my grandmother Servet Çopuroğlu for lightening my path, for making me always smile and for their endless support.

I would like to express my thanks to Tevfik Yüksel and Bülent Taşkeli for their invaluable support and sharing their wisdom. I feel lucky for not only working with them but also being a member of the printed circuit board production family at Aselsan.

The author is thankful to Onur Yurtsever, Mehmet Kaptan, Saygın Aras, Osman Karslıoğlu, Mert Oymak, Başar Cağlar, Orçun Ergün, Hilal Demir Kıvrak, Arzu Kanca and Mukaddes Can for their support and gorgeous conversations. I know that each of them deserves the best for everything.

I am thankful to UNAM and METU Metallurgical and Materials Engineering Department for providing SEM facilities. Financial support was provided by TUBITAK through 1002 project 108M631.

With the support of all those mentioned (and unintentionally forgotten), I was able to make my personal contribution to alternative energy technologies in the world. I know that journey of a thousand miles must begin with a single step and I am grateful to all helping me to the first step.

TABLE OF CONTENTS

LIST OF TABLES

TABLES

LIST OF FIGURES

FIGURES

LIST OF SYMBOLS

V	Voltage, V
i	Current, mA
j	Current density, mA/cm^2
P	Power, mW
R	Resistance, ohm
P_{MPP}	Maximum power point, mW
V_{MPP}	Maximum voltage point, V
i_{MPP}	Maximum current point, mA
FF	Filling factor
V_{OC}	Open circuit voltage, V
I_{SC}	Short circuit current, mA
J_{SC}	Short circuit current density, mA/cm^2
TCO	Transparent conducting oxide
PV	Photovoltaics
DSSC	Dye sensitized solar cell
toe	Tons of oil equivalent

CHAPTER 1

INTRODUCTION

1.1. THE ENERGY NEED

Today, most of worldwide energy use is based on fossil fuels. It is expected that world demand for fossil fuels will exceed annual production soon and shortages of fossil fuel may cause international economic and political crises and conflicts. Moreover, it is known that combustion of fossil fuels releases emissions to the environment and the combustion products have not only local but also global effects. World public opinion, declared by international and national institutions and other organizations, are increasingly aware of these risks and they are pointing to a need for a fundamental transform of main energy source from fossil fuels to renewable energy sources. Even today, renewable energy sources provide many opportunities to fulfill the energy demand. According to World Economic Council Report [1], the share of renewable energy sources is expected to grow by 56% over the next 24 years. A major contribution to this transformation can be expected to come from solar energy. In several regions of the world, we can see the signs of this transformation, not only at the technological level, but also at political levels.

Thus, solar radiation which is the earth's prime source of renewable energy becomes more attractive each year to satisfy the energy demand. Although the photovoltaic (PV) power generation is still the most expensive solar technology, cheaper systems are available and many stand alone applications can be seen in many areas. Actually, solar applications are already taking place in the building construction industry, in particular with water heating. Roofs and walls are already becoming the potentially largest area in which PV and thermal systems are installed to collect solar radiation.

With its rapidly growing economy and with a population of more than 70 million people, Turkey is in the World's 20 largest economies. The energy demand of Turkey has increased rapidly as a result of social and economic development. Also, it is known that Turkey is an oil importer country and has to meet its energy demand on its own sources for a sustainable growth. As far as it is believed that Turkey is not lucky by fossil fuels, potentials for renewable resources have to be examined. At this point, it should be emphasized that Turkey is in the solar rich area. According to the International Energy Agency [2], the daily average solar intensity is 3.6 kWh/m^2 in Turkey. Moreover, it is reported that 10 million m^2 installed solar thermal collectors indicates the positive attitude of Turkish people towards solar energy. Consequently, solar energy provides a great potential to supply the energy demand of Turkey.

Turkey is in between 36-42 north latitude and in the middle of a solar rich area. According to Ministry of Energy and Natural Resources [3], Turkey has an average of 2609 sunshine hours/year and it changes from one region to another. Also, it is given in the report that the most sunny area is exposed to 3016 hours and the least sunny area is exposed to 1966 hours. Also in the report, the seasonal changes

over the country was given to be between 5.9 kWh/m^2.day to 1.5 kWh/m^2.day [3]. In addition to these, the regional solar potential of Turkey is given in Table 1.1 to clarify the regional solar potential changes better.

Table 1.1. Solar potential of Turkey by regions [4]

	Yearly		**July**		**December**	
Region	MJ/m^2.d	kW/m^2	MJ/m^2.d	kW/m^2	MJ/m^2.d	kW/m^2
South East Anatolia	14.3	0.477	23.0	0.767	8.5	0.283
Central Anatolia	13.9	0.463	21.7	0.723	5.5	0.183
Mediterranean	13.7	0.457	21.6	0.720	4.8	0.160
Aegean	13.5	0.450	21.7	0.723	5.0	0.167
East Anatolia	13.4	0.447	20.0	0.667	4.9	0.163
Marmara	10.9	0.363	17.8	0.593	4.0	0.133
Black Sea	10.3	0.343	15.3	0.510	4.7	0.157

According to Turkish Industrialist's and Businessmen's Association [4], it was reported that Turkey's capacity of producing thermal energy from solar energy is 120,000 toe/year in 1998 and it is predicted that in 2020 and 2025 this production will be 745,000 toe/year and 932,000 toe/year respectively. Also in the same report,

gross potential for solar energy is given as 80.000 Mtoe/year. It is reported that most of the thermal energy production by using solar energy is located especially in the south part of Turkey.

1.2. SOLAR CELLS

There are many solar cell types and applications in the world for finding a solution to energy problem. The most preferred solar cell type is conventional silicon solar cell which is also known as photovoltaics. In conventional silicon solar cells, two types of crystals are used. One is the n-doped which has a free electron to move and the other is p-doped which has a lack of electron. When these two crystals are combined, the free electron tends to move from n-doped crystal to the p-doped crystal to fill the missing electron which is named as electon hole. As soon as solar radiation hits the surface of the cell, photons in the light excites the valence electrons of p-doped crystals and this photoexcited free electrons move to the n-doped crystal. Then the electon again transferred from n-doped crystal to p-doped crystal to fill the electon hole. Thus, the current is produced by using the solar radiation. A typical crystalline silicon cell composed of two kinds of silicon layers. The first one is the layer where sun light hits which is negatively doped with phosphorus and the second one is the layer which is positively doped with boron. At the boundary layer of two layers, charge separation occurs. Besides, a metallic contact is used on the front and back sides of the cell to take the power to outside of the cell.

There are some problems in PV technology to be solved. For instance, some of the freshly ejected electrons from p-doped area are taken from the other p-doped crystals in the system. Surely this is

one of the major factors for inefficiency of conventional PV solar cells. Besides, because some photons have a higher energy than the required energy for photo excitement, remained energy transformed to heat after the photo excitement. Also, silicon is an expensive material and many practical obstacles exist to reduce the cost of processing silicone [5].

Besides, a stand alone traditional PV system has the following components: PV module, charge controller, rechargeable battery, load, inverter. Generally, PV systems need some energy storage systems because the electricity produced by the PV modules can not be consumed immediately. Most common semiconductor material is silicon but gallium, cadmium, tellurium and copper can be used in photovoltaic cells also. Many types of PV exist but crystalline solar cells are the most preferred one in worldwide market.

In 1991, the first dye sensitized solar cell (DSSC) with a conversion of 7.1% was announced [6]. DSSC is a system which mimics the photosynthesis in terms of transforming the solar energy to another form of energy which is electricity. It is announced in 2005 that a %11 efficiency is attained for a DSSC [7]. A typical DSSC achieved more than 10% sunlight to electrical power conversion efficiency [8] while 15-17% conversion efficiency has been attained by typical commercial silicon solar cell modules [9]. Note that 1% efficiency is a typical value for tropical forest ecosystems, [10] and 13% for the calculated limit for natural photosynthesis [11].

Mainly, a typical DSSC is composed of a wide band gap oxide semiconductor, an electrolyte, a sensitizer (dye) and a counter-electrode as it is shown in Figure 1.1. On the anode side of the cell, dye is adsorbed on the semiconductor oxide which is sintered on Transparent Conducting Oxide (TCO) glass. On the cathode side,

there is another TCO with a catalyst coating over it. A redox electrolyte fills the gap between two TCO glasses. In general, semiconductor of choice is titanium dioxide, electrolyte couple is iodide/triodide (I^-/I_3^-), counter electrode is platinum and the dye is the ruthenium base one [12]. The working principle of a DSSC is as following; the sensitizer is photo excited by adsorbing the incident solar rays. After the sensitizer is excited, it injects its electron to the conduction band of the oxide which is anchored to the sensitizer. Then, excited sensitizer is regenerated by the electron from electrolyte which is a redox couple which is typically iodide/triodide in an organic solvent. The oxidized dye is regenerated by the taking electron from the iodide and forming triiodide. Next, the iodide is regenerated by the triiodide at the counter-electrode. Cycle is completed by the electron migration between TiO_2 (anatase) and counter-electrode which is usually Pt coated TCO. The electron cycle of the system is showed in Figure 1.1 [8, 13].

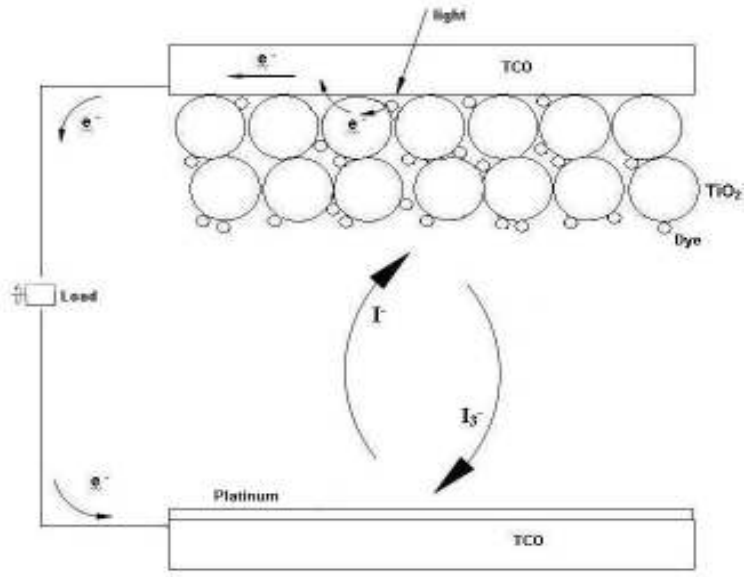

Figure 1.1 Operating principle of the DSSC

The electron cycle in the cell was studied by Gratzel, 2001 [14] and is given in Figure 1.2.

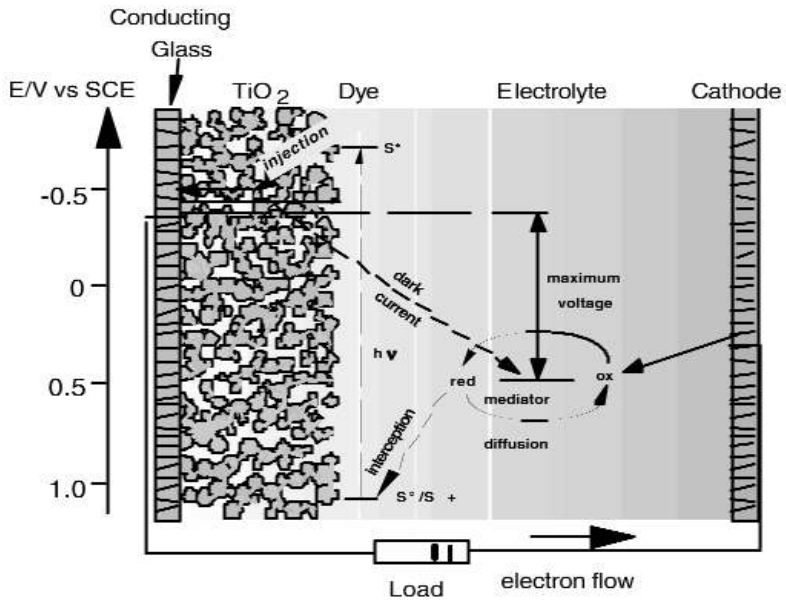

Figure 1.2. Electron cycle in the DSSC [14]

For harvesting the solar energy, a sensitizer is adsorbed on a semiconductor oxide as mentioned before. However, a monolayer of dye can absorb very limited amount of solar energy due to the limited cross section area of the dye molecules. Also, multilayer application of dye is not a solution because the layers filter the solar rays. Thus, another strategy is used to increase the light capture cross section. Mesoporous nano size TiO_2 is used to increase the total surface area. It is emphasized that, solar rays are absorbed by the dye covered nano-oxide sponge much better due to the increase of the surface area by the use of such nano particles. Surface gets 1000 times larger for a 10 μm mesoporous nano-thick oxide film which means that the efficiency in sunlight captured by dye covered oxide

gets much larger [14]. Although alternative wide band gap oxides such as ZnO and Nb_2O_5 can also be used as semi-conductor oxide, TiO_2 is the most preferred one because it is abundant due to the large scale use in paint industry, non-toxic and relatively inexpensive. Note that mesoporous nano scale anatase particles are used to increase the area which is exposed to sun light to raise the efficiency. There are two main regeneration phase systems in a DSSC which are solid state DSSC and liquid state DSSC. DSSC using a liquid electrolyte includes a redox couple to regenerate the sensitizer. Electrolyte is composed of an organic solvent and a I^-/I_3^- redox couple. The aim of using electrolyte is the regeneration of DSSC. I^- ion in the electrolyte regenerates photo excited dye molecule. Voltage produced by DSSC is the difference between the chemical potential of the titanium dioxide (Fermi level) and the redox potential of the electrolyte. Generally, KI or LiI and I_2 are dissolved in an organic solvent, usually acetonitrile (ACN) or ethylene glycol . The main reactions proceeding in the system are described by Smestad [15] and also by Hauch and George [12] and they are given by the equations from (1-1) to (1-4).

Dye molecule is photo excited by the equation (1-1).

$$\text{Dye} + \text{light} \rightarrow \text{Dye}^* \qquad (1\text{-}1)$$

Then, it ejects its electron to the conduction band of the semi-conductor oxide as it is shown in equation (1-2).

$$\text{Dye}^* + TiO_2 \rightarrow e^- (TiO_2) + \text{Dye}^+ \qquad (1\text{-}2)$$

Dye molecule is reduced by the electrolyte couple with the reaction given below:

$$2\ \text{Dye}^+ + 3\ I^- \rightarrow\ I_3^-\ + 2\ \text{Dye} \qquad (1\text{-}3)$$

Then, at the cathode side of the cell which is usually Pt, iodide is regenerated by taking the electron.

$$I_3^- + 2\,e^- \rightarrow 3\,I^- \qquad (1\text{-}4)$$

Surely the charge transfer resistance of Pt and diffusion constant of triiodide are also important parameters for the regeneration process [12, 15].

Counter electrode or cathode, is used to regenerate the electrolyte couple which in turn, regenerates the photo excited dye molecule. In other words, counter electrode is responsible for catalytic cathodic reduction of triiode to iodide. Although many other materials like carbon and conductive polymer are tried, platinum is still the most preferred material because it shows high catalytic activity for triiodide / iodide reduction and its light reflectivity is at an acceptable amount. Many platinum coating techniques are used like electon beam evaporation, sputtering, thermal decomposition, electrodeposition and thermal treatment for platinization of the cathode.

The efficiency of a DSSC strictly depends on the sensitizer of choice. Following properties for a sensitizer are quite important. Absorption spectrum of the dye is critical because dye should adsorb the visible light. Also, the redox properties of the ground state and excited state of the dye molecule have to be examined. Because both electron transfer between sensitizer and electrolyte and between sensitizer and TiO_2 strictly depends on this criteria. Besides, anchoring ability of dye to the TiO_2 affects the electron transfer. Energy levels of the dye and semi conductor oxide must be proper such that electron can be transferred from dye molecule to the semi conductor oxide as it is described in Figure 1.2. Carboxyl or hydroxamate groups can anchor the dye molecules to TiO_2 well so electron transfer from dye

molecule to the conduction band of TiO_2 molecule can be made successfully. In addition to these, dye should be regenerated fast enough after loosing its electron. Finally, it should be stable for 20 years of exposure to natural light for being economically feasible [8]. According to the criteria given above, Ru and Os based sensitizers are the best molecules reported up to now. General structure of a typical sensitizer is $ML_2(X)_2$, where L 2,2'-bipyidyl-4,4'-dicarboxylic acid, M is Ru or Os and X is halide like cyanide, thiocyanate or water. Note that most famous dye N3 was found in 1993 and ruthenium complex of it is cis-RuL_2-$(NCS)_2$. Nowadays, a better one is found which is called as black dye which adsorbs the near-IR is better than N3 [14, 16, 17].

1.3. SOLAR BASICS

Intensity of the solar radiation depends on the distance between sun and earth. Because the distance changes between 1.47 x 10^8 km and 1.52 x 10^8 km, the intensity changes between 1325 W/m^2 and 1412 W/m^2. Also, not all of the solar irradiation reaches the surface. The main reasons for decreasing the solar intensity are the reflection from atmosphere, adsorption by atmosphere, scattering by dust and pollutants in the air. In good weather, on the average 1000 W/m^2 solar intensity reaches to the surface at noon. Also solar altitude is important. When the altitude is perpendicular to the surface to the earth, solar radiation takes the shortest path to the surface and yields more energy to the surface; as the angle changes from 90^o, path increases which cause a decrease in energy reaching the surface. Thus, air mass (A.M.) factor is used to define the relationship between solar altitude height and A.M. For Europe, A.M. 1.5 is used as the average annual value.

For getting a more specific and precise solar radiation values, pyranometers, photovoltaic sensors and satellite images can be used. Pyranometers are the sensors that measure solar radiation of a planar surface. It gives very accurate results but it is slow. Photovoltaic sensors are cheaper but less sensitive than pyranometers and they can not measure all the spectrum of the light. Finally, satellite images can be analyzed by software's to estimate solar radiation hitting the earth.

These intensity measurement systems can also be used to increase the efficiency of the solar cells. For instance, energy yield from the sun increases if the surfaces of the PV panels are always perpendicular to the sun. Thus, electromechanical or hydraulic tracking system is used to move the panel surfaces according to the movement of the sun. By using this tracking system, 50 % energy yield increases in summer and 300% in winter compared to horizontally aligned panels.

In order to compare different cells, current-voltage curves of the cells are used. For overall cell efficiency, the most important parameters are open circuit voltage (V_{oc}), short circuit current density (J_{sc}) and the maximum power point (P_{MPP}). Also voltage at the maximum power point (V_{MPP}) and current at the maximum power point (i_{MPP}) can be used. Another important parameter is the filling factor (FF) which is defined as the ratio of maximum power of the cell found from voltage-current curve to the theoretical maximum whose formula is given by equation (1-5).

$$FF = P_{MPP} / V_{oc} \times I_{sc} \qquad (1\text{-}5)$$

These parameters are important for calculating the efficiency of the solar cell. The following equations are valid:

$$R = V / i \quad (1\text{-}6)$$

$$P = V \times i \quad (1\text{-}7)$$

Efficiency of a solar cell (η) is expressed as the ratio of maximum power point to solar irradiance hitting to the panel surface.

$$\eta = (P_{MPP}) / (E \times A) = (FF \times V_{oc} \times I_{sc}) / (E \times A) \quad (1\text{-}8)$$

where A is the effective area of the cell and E is the solar irradiance. The current density (j) is another parameter that is used frequently for calculations and defined as given in (1-9)

$$j = i / A \quad (1\text{-}9)$$

For instance, 10.6 % efficiency is reported by using N3 dye at A.M. 1.5 where E is 1000 W/m^2 [17]. Also some efficiency values from the literature are given in Table 1.2.

Table 1.2. Some examples of performance parameters of DSSC

Focus of the study	**V_{oc} (V)**	**j_{SC} (mA/cm^2)**	**Efficiency (%)**
Ionic electrolyte [18]	0.55	9.40	2.4
Thermal decomposition of Platinum [9]	0.70	13.87	6.3
Electrodeposition of Platinum [9]	0.73	15.38	7.6

The current is linearly proportional to the solar irradiance. A straight line is expected between the current and solar irradiation. Voltage increases with solar intensity sharply up to 100 W/m^2 and still increases slightly after 100 W/m^2 with the intensity [5].

CHAPTER 2

LITERATURE SURVEY

Because the energy demand of the world increases each year, the importance of the renewable energy sources like solar energy increases more and more each day especially for the countries in the solar rich region like Turkey. Many solar cell products are already in the market and new ones like DSSC are coming. DSSC is a new type of solar cell that mimics the photosynthesis. It is much cheaper than conventional solar cells and its production is simpler than photovoltaics. Numerous studies have been conducted for each part of the DSSC to increase the efficiency. Some studies are summarized in this chapter.

2.1. SEMICONDUCTOR OXIDE

Mesoporous nano sized anatase particles are typically prepared by sol-gel procedure. The main advantage of this procedure is that it is quite easy to adjust the particle size, nanostructure and porosity of mesoporous nano-oxide film. Process is strictly temperature dependent. Basically sol gel procedure involves the following steps. Firstly, amorphous precipitate of titanium dioxide (TiO_2) is produced by hydrolysis. Then, the sol was produced by peptisation in acid or alkaline water. Next, the sol was left in an autoclave for Ostwald

ripening. It is noted that the resulting TiO_2 particles are in the form of anatase or rutile according to the parameters used in sol-gel procedure. A standard sol is treated for about 450 ^oC to establish a strong contact between the particles and it is reported that resulting film thickness is typically 5-20 μm and TiO_2 mass is about 1-4 mg/cm^2, porosity is 50-65 % [13, 14].

It is known that choosing the semiconductor is the heart of the process and some requirements must be satisfied by the semiconductor. For instance, mesoporous sponge structured oxide films are needed to be n-doped to conduct electrons. Also, it has to be a wide band gap oxide. Many materials like TiO_2, ZnO, SnO_2 and Nb_2O_5 are the wide band gap oxides and have been investigated for years. TiO_2 (anatase) become the semiconductor of choice because it meets the all requirements mentioned above. Moreover, it is cheap, not toxic and easy to produce [8]. Also there are studies on semiconductors which are doped with other metals to increase the efficiency. For instance, Keis *et al.* announced that a higher efficiency is obtained for Al-doped ZnO films than the undoped ones. It is stated that Al doping process cause more free electrons results in better conductivity to increase the efficiency [20].

There are some optical enhancement studies focusing on increasing the light capture capabilities of the DSSC. For example, titania inverse opals are covered on the nanocrystalline TiO_2 layer such that it forms a bilayer of semiconductor oxide. A polymer film is used to prevent filling of titania inverse opals into the mesoporous structure of nanocrytalline TiO_2 in such kind of systems. Lee *et al.* announced that addition of titania inverse opals to nanocrystaline TiO_2 layer increase the efficiency from 6.5 to 8.3 % under the anode side illumination [21].

There are many studies for making the TiO_2 deposition more proper for mass production. For instance, sputtering process is thought to be one of the best candidates for mass production. Magnusson *et al*. announced that 2.34 mA/cm^2 short circuit current density is attained for 9.7 μm film thickness prepared by sputtering instead of sol-gel procedure. Also they announced that maximum open current voltage value is 0.4-0.6 V. Moreover, it is stated that a higher short circuit current value is attained for sputtered deposition than the sol-gel prepared film for the same TiO_2 thickness [22].

2.2. SENSITIZER

Sensitizers are the chemicals which are used to adsorb the visible light and inject their electron to the semiconductor oxide to start the electon transport cycle in the cell. Most typically, Ru based dyes are preferred as sensitizers. For instance the standard dye is tris (2,2'-bipyridyl, 4,4'-carboxylate) ruthenium(II) was used by Gratzel and his co-workers in 1991 [6]. There are numerous studies on sensitizers to increase the efficiency of the DSSC. For instance, a cis - dithiocyanato bis (4,4A - bicarboxy - 2,2 A – bipyridine) ruthenium (ii) complex gives a solar to electric power conversion efficiency of 10% at AM 1.5 condition. For improving the efficiency, sensitizer has to be more sensitive to red and near-IR region of the light. Nazeeruddin *et al.* announced that a black trithiocyanato–ruthenium (ii) terpyridyl complex where the terpyridyl ligand is substituted by three carboxyl groups is very efficient over the whole visible range and also it gives good response to the near-IR region up to 920 nm [23].

Besides, boradiazaindacenes (BODIPY) based dye is studied as sensitizer because these molecules are useful fluorescent labels for

biomolecules. Ela *et al.* announced that system gives 1.66% efficiency. Also, 4.03 mA/cm^2 short circuit current and 0.562 V open circuit voltage are attained [24].

Even though Ru based dyes are the most preferred ones because they provide the highest efficiencies, it is hard to synthesize them. It is also possible to use some kind of natural fresh fruits like raw berries and strawberries as sensitizers but their efficiencies are quite low and these dyes still require further purification processes. There are some studies on natural dyes such as chlorophyll derivatives and on the average 2.6% efficiency and current of 9.4 mA/cm^2 is announced by Kay *et al.* [25].

Successive adsorption of the light in a wavelength range from visible to IR is quite important to increase the efficiency of the cell. To achieve this aim, not only new sensitizers having larger adsorption ranges are developed but also co-sensitization of dyes are used at the same time such that one dye adsorbs blue part of the visible spectrum and the other adsorbs the red part and near IR spectrum.. The aim of using different dyes in the same DSSC is to increase the efficiency by making the DSSC compatible with a wider light spectrum. For example, Kuang *et al.* reported that the co-sensitization of dyes yields 6.4% efficiency under A.M. 1.5 sunlight [26]. In co-sensitization process, a sequential impregnation of the sensitizers is applied to the anode side of the DSSC.

2.3. ELECTROLYTE

Many redox couples are studied to find the most suitable electrolyte system for DSSC. For instance, potassium iodide was mixed with iodine in water-free ethylene glycol by Smestad [15]. A few drops of

electrolyte were added to edge of the DSSC and it was soaked by capillary force. In another study conducted by Hauch and George, DSSC was filled with the electrolyte of lithium iodide and iodine in acetonitrile [12].

Besides the studies on the redox couples, some studies for decreasing the loss of electrolyte in the DSSC were also conducted. For instance, the electrolyte may leak by the time because many sealing difficulties can be encountered during assembly, solid state DSSC was developed to eliminate the sealing problem. A typical solid state DSSC is composed of a n-type semiconductor, dye and a p-type semiconductor which means that sensitizer sandwiched between the two semiconductors. It is emphasized that preparing a solid state DSSC by using a solid electrolyte will be improper because of the low electron mobility. Thus, a choice of p-type semiconductor which is replaced with the electrolyte will be a better solution. Tennakone *et al.* stated that CuI is the best p-type because it has a high band gap, transparent and not expensive. Tennakone and his co-workers announced that 2.5 mA/cm^2 and 375 mV is attained under 800 W/m^2 light intensity which correspond to 0.8% energy conversion efficiency [16].

In a typical DSSC, electrolyte can leak by time as it is mentioned before. Another solution rather than using solid state DSSC is using an electrolyte having a higher viscosity to decrease the rate of leakage. For instance, viscosity of typical ionic liquids is about 100 times larger than that of acetonitrile which is a typical organic solvent in DSSC. The main advantages of ionic liquids are non-volatility, non-flammability and high ionic conductivity. Kawana and his co-workers prepared a DSSC having EMImDCA as ionic liquid and announced a efficiency 5.5% under 1000 W/m^2 light intensity [18].

Also, there are studies on the electron transport kinetics. For instance, Peter *et al*. stated that in an efficient cell, back transfer of electrons, which are resulted from photo injection, has to be as slow as possible such that electrons can accumulate in the oxide and generate voltage. However, regeneration process at the cathode side must be fast to prevent production of a large over potential loss when the current flows [27].

2.4. COUNTER ELECTRODE

Counter electrode is another critical component of a DSSC. The main purpose of the counter electrode is the reduction of triiodide. The reduction reaction rate at the cathode is important because after the reduction of triodide, iodide is formed which is used to regenerate the oxidized dye molecule at anode side of the cell. For having a feasible DSSC, cell must be stable for 20 years and this can be accomplished only by having enough regeneration cycles according to Hagfeldt and Gratzel [8]. For having a feasible cell, reaction at the anode side must be slow and reaction at the cathode side which is the counter electrode must be fast. Counter electrode is near the equilibrium potential of the redox couple but anode side is far from the equilibrium potential. This phenomena creates a voltage difference in the DSSC causing tri-iodide reduction [28, 29]. Although many materials like platinum, carbon, conductive polymers are used as counter electrode platinum is the still catalyst of choice. Platinum is a better catalyst for iodide/triiodide redox couple. Also light reflection value of platinum is also higher than carbon coating which causes reflection of more light into the cell. Because the counter electrode is the heart of the regeneration process in DSSC, there are many studies on it.

Weak adhesion of the platinum and corrosion of the platinum by the electrolyte are two important problems to be solved in a DSSC and stability of the platinum strictly depend on platinization method. Also, for increasing the efficiency and having longer cell life, many platinum coating techniques are tried. There are many studies for comparing the platinum coating techniques. For example, Kim *et al.* stated that pulse electrodeposited Pt has higher active surface area than direct current electrodeposited Pt coating which was found by cyclic voltammetry curves. Moreover, they showed by using SEM images that Pt structures differ considerably from each other when different techniques are applied. Also, the short circuit current was increased from 10.34 mA/cm^2 to 14.11 mA/cm^2 and efficiency was increased from 3.68% to 5.03% by changing the coating method from direct current to pulse deposition. Besides, Kim and his co-workers concluded that pulse current method provides better particle size control, adhesion and uniformity in film morphology [30].

Another comparison study for the comparison of sputtering, thermal decomposition and electrodeposition techniques were performed by Yoon *et al* [9]. Thermal decomposition was used with $H_2PtCl_6.2H_2O$ in 2-propanol, sputtering was achieved by deposition of Pt on conducting glass by a sputtering machine and electrodeposition was made by using potentiostat/galvanostat assembly. They found that electrodeposition gives more active surface area and its efficiency is better than sputtering and thermal decomposition. When the microstructures were examined by using SEM images, the following results were found; granules with imprecise shape in thermal decomposition well shaped polyhedrons in sputtering and spherical or elliptical granules in electrodeposition. Moreover, they found that 0.1% efficiency is attained without any Pt on the glass [9].

Also there are many studies on the kinetics of the reactions proceeding over platinum. For instance, Hauch and George stated that rate determining step among the reactions in the DSSC is the oxidation of iodide on the platinum. Besides, it was emphasized in the study that adhesion of platinum over glass is critical because it may cause back current if platinum sticks on anode side of the DSSC. Also, a platinum thickness optimization was made in the study and they found that as the platinum thickness increases, the charge resistance decreases because the increase in the effective area shown in SEM images. Also, they found that only 2 nm was enough to decrease resistance considerably [12].

Papageorgiou *et al*. prepared a platinized surface by thermal decomposition of H_2PtCl_6 at 380 ^oC for 10 minutes on SnO_2 coated glass substrate and they stated that process yields platinum nanoclusters having a particle size up to 20 nm and its performance was better than electrochemically deposited platinum because of having lower charge transfer resistance. Also, Papageorgiou and his coworkers showed nano size platinum clusters which were connected to SnO_2 by using HRTEM. Besides, Papageorgiou and his coworkers stated that low platinum loading like 3 $\mu g/cm^2$ caused a transparent cathode appearance but it was enough to run the DSSC. Moreover, they emphasized two important conclusions. First, at high platinum loading amounts, current increased because the increase in active surface area dominated the negative effects of in larger particle sizes on current. Secondly, current value gives a peak by increasing annealing temperature and this peak was affected by the platinum loading to the cathode [31].

Bönnemann and his coworkers stated that higher platinization temperature leads a broader particle size distribution according to the

TEM images. Besides, it is known that +2 and +4 oxidation state of platinum provides lower catalytic activity than zerovalent platinum for triiodide reduction reaction and Bönnemann *et al*. reported that 76% platinum precursor was at the zero valence state and the remaining part in at the +2 and +4 oxidation state when platinization was applied by thermal decomposition under 380 ^{o}C [32].

Khelashvili *et al*. stated that thermal decomposition at 380 ^{o} C, yields 76% zero valent platinum and thermal decomposition at 580 ^{o} C was needed to transform the H_2PtCl_6 precursor totally to zero valent sate. This is a very critical result because it is known that at the zero valent state, platinum is more active for triioide/ioide reaction. Also Khelashvili and his coworkers confirmed that as the annealing temperature increases, platinum particles agglomerates more but particles size distribution gets broader. Besides, they confirmed the results of Bönnermann *et al.* such that higher annealing temperature cause an increase in platinum cluster sizes with a broader particles size distribution [33].

These findings are in good agreement with the supported catalyst literature. For the most supported precious metal catalysts, active sites of the catalyst are characterized by gas phase hydrogen and carbon monoxide chemisorption. For liquid phase systems, Kivrak *et al.* made a comparison of all terrace and defect sites and claimed that nearly all reaction proceeds at the defects of the metal particles located at the edges and corner sites. It is also known that the defect sites are related with the particle size of the catalyst. Then, playing with the particle sizes changes the defect size amounts and it effects the reaction rates [34]. The edge and corner site densities increase as the particle size decreases. Uner and Uner showed that because calcination temperature changes the particles sizes, it is possible to

change the defects by changing the temperature and microcalorimetry can be used to make characterization [35].

CHAPTER 3

MATERIALS AND METHODS

There are many studies on each component of the DSSC to increase the efficiency, numerous materials and chemicals have been tried and many equipments, methods and characterization techniques have been developed for years. Because the aim of this study is investigating the effects of the platinum particles sizes on the cell efficiency, standard methods and well known materials were chosen for the main components of the DSSC. The materials, methods and techniques are given in this chapter.

3.1.MATERIALS

Transparent Conducting Oxide (Solaronix) having the dimensions of 5cm x 5m and thickness of 2.2 mm was used as conducting glass. It has a fluorine doped tin oxide (SnO_2:F) layer on one side which is also known as FTO glass and its transmission is reported as more than 80 % from 400 to 700 nm wavelength of the light. Ti-Nanoxide T20 (Solaronix) was the choice of anatase. It is a paste containing 11 weight % anatase with uniform particle diameter of 20 nm. Ruthenium 535 (Solaronix) whose chemical name is cis - bis (isothiocyanato) bis (2,2'-bipyridyl-4,4'-dicarboxylato) - ruthenium (II) was the choice of sensitizer. Plasitol (Solaronix) which is alcohol

based solution of platinum precursor was used for coating counter electrode. Potassium iodide, iodine and ethylene gylcol (Merck) were used for preparing electrolyte couple. Also, pure ethanol (Merck) was used for cleaning purposes.

3.2. PREPARATION OF THE DSSC

3.2.1. Deposition of TiO_2

Because it is very important to work with a fingerprint free transparent conducting oxide (TCO), always gloves were used and TCO was cleaned with alcohol prior to use. TCO was heated to 50 ^oC at the beginning of the process to increase the adhesion. Then four pieces of 0.5 cm wide Scotch 3M adhesive tape were applied on the edges of the conductive side of the TCO glass. The reason for applying tapes was preparing a mould such that nonsintered TiO_2 has always same area and thickness for all samples. Then 1.5 gr Ti Nanoxide T20 was dropped on the conductive side of the TCO after the conductive side of the TCO was checked by the multimeter. Then, the TiO_2 paste was uniformly distributed over the TCO by using a glass rod. Next, the tapes were removed from the glass and plate was sintered between an air blower at 500 ^oC and a hot plate at 350 ^oC for 30 min such that hot air gun was 30 cm above the TiO_2 coated TCO. Color of TiO_2 becomes brown in the middle of the sintering process and then its color changes to the brownish-white. This color remained till the end of the sintering process.

3.2.2. Impregnation of Sensitizer

For preparing the dye solution, Ruthenium 535 was dissolved in ethanol in a ratio of 1:5. Solution was heated up to 60 ^oC and TiO_2

coated TCO was put in a face-up manner into the solution. After 5 hours of impregnation, the back side of the TCO was checked for uniform coating of the sensitizer such that no white area was observed.. After the impregnation, electrode which was anode of the DSSC was dried in the air.

3.2.3. Preparation of Counter Electrode

The platinization procedure given by Solaronix [36] was applied because the material was taken from Solaronix. Actually, this method is simply called thermal decomposition which is most widely used platinization procedure. Plasitol was applied on the surface by using a brush. All TCO glasses were sintered at 400 ^{o}C for 5 minutes for decomposition which was the minimum required calcination condition according to the procedure. In addition to this step, further sintering process, whose details are given in Table 3.1, was applied to change the surface morphology. All sintering processes were applied in NEY 525 Series 2 oven equipped with a time controller and thermocouple.

Table 3.1. Sintering parameters of counter electrodes

Sample	Calcination process	Sintering process
1	5 minute at 400 ^{o}C	-
2	5 minute at 400 ^{o}C	30 minute at 450 ^{o}C
3	5 minute at 400 ^{o}C	30 minute at 500 ^{o}C
4	5 minute at 400 ^{o}C	30 minute at 550 ^{o}C

3.2.4. Electrolyte Preparation

0.5 M potassium iodide and 0.05 M iodine were mixed in pure ethylene glycol as described by Smestad [15]. The resulting solution was stored in a dark colored glass bottle. 1 ml of electrolyte was added to the cathode of the DSSC and waited until it was ensured that whole cell was wetted before completing the assembly of DSSC.

3.2.5 Assembling the DSSC

First, the conductive side of the anode was placed on top of conductive side of the counter electrode. The alignment was made such that one uncoated side of the TiO_2 was in an offset position. These offset points served as contact points for multimeter during measurements. Finally binder clips were used to keep the DSSC assembled. The assembly procedure of Smestad, 1998 [15] was followed, the assembled cell looked similar to the schematics given in Figure 3.1. As it was mentioned before, alligator clips were connected to multimeter during measurements.

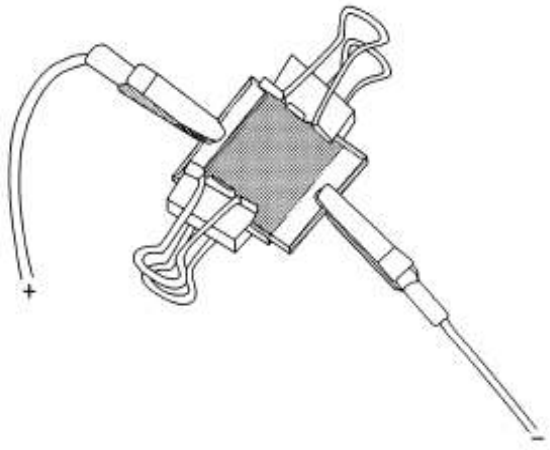

Figure 3.1. Representative illustration of assembled DSSC [15]

3.3. CHARACTERISATION

SEM measurements were made by FEI Quanta 200 F in National Nanotechnology Research Center (NNSR) at the Bilkent University. EDX mapping and further SEM micrographs were taken from FEI Nano-SEM at METU Metallurgical and Material Engineering Department. SEM micrographs were taken for both top side and cross sectional side of the TCO samples. Moreover, image analysis of the micrographs were made by MedCalc Digimizer 3.7.0.0 which is a professional image analyzer which has the ability of finding average length, perimeter and area of particles from the SEM images. Also, all current, voltage and resistance measurements were made by Brymen BM810a multimeter.

3.3. MEASUREMENTS

The voltage-current measurements were done by the multimeter and the resistances used were given in Table A.1 in Appendix A. The measurement setup is shown in Figure 3.2. During the measurements, it was assumed that multimeter had an infinite resistivity and battery of it was ideal. The calculation details for voltage-currennt data was given in Appendix B.

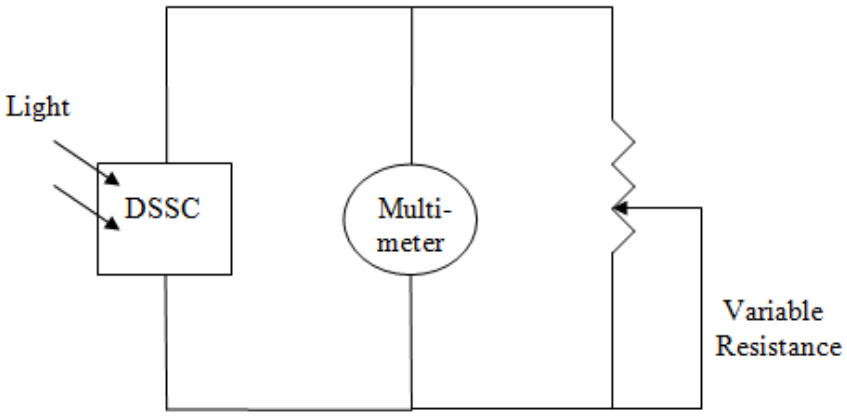

Figure 3.2. Schematic illustration of current-voltage measurement setup

Measurements were done as follows: DSSC was put in to the Atlas Suntest CPS + Solar Simulator which has a 300 W Xenon lamp. Positive electrode of multimeter was connected to the counter electrode of the DSSC and negative electrode of multimeter was connected to the TiO_2 electrode.

Standard measurements require 1000 W/m^2 solar intensity. Because 1000 W/m^2 was beyond the upper limit of Atlas Suntest CPS +, 650 W/m^2 was chosen as the solar intensity. Then, solar simulator was set to 650 W/m^2. A set of resistances given in Table A.1 in Appendix A were selected for using the same loads for all measurements. The photograph of the setup is also given in Figure C.1 in Appendix C.

A sample calculation for current, power, filling factor and efficiency is given in Appendix B and a brief calculation procedure is as follows: Solar simulator was started at least 15 minutes in advance to obtain a constant light intensity. The resistance was adjusted to a certain

value given in the Table A.1 in Appendix A. Then, voltage was read from multimeter and corresponding current was calculated by equation (1-6). Then the same procedure was repeated by changing the resistance to next value in Table A.1. Finally, a current-voltage figure was plotted for one counter electrode according to collected data. Then, the whole procedure was repeated for a new DSSC having a different counter electrode prepared at different sintering conditions given in Table 3.1. Next, by using the current-voltage values, the power values were calculated by using equation (1-7). Then, power-voltage curves were plotted. The FF (filling factor) values were calculated by using maximum power points (P_{MPP}) in power-voltage curve and calculated by equation (1-5). Finally, efficiency values were calculated by using equation (1-8).

CHAPTER 4

RESULTS AND DISCUSSION

Because the increasing energy demand is one of the most important problems in the world, there are many studies on renewable energy sources like solar energy. Dye sensitized solar cell is one of the best candidates among the solar energy technologies because it is cheap, its efficiency does not decreases as the temperature of the cell increases and its production is not as complicated as the photovoltaics. Eve though its efficiency reached 11% and it becomes commercial, further improvements are needed to increase the efficiency to decrease the cost. In this study, it is aimed to investigate the role of the platinum particle sizes on the efficiency because platinum is one of the most expensive components of the cell.

As it was described in Chapter 3, anode side of the DSSC was prepared by sintering TiO_2 on a TCO and ruthenium based dye was adsorbed on the TiO_2 coated TCO. Cathode side was coated by platinum and different sintering conditions given in Table 3.1 were applied to make morphological changes on the cathode surfaces. Next, KI and I_2 were dissolved in ethylene glycol and the solution was added to the cell. Finally, cell was combined by binder clips. After the measurements described in Chapter 3, the results which are given in this chapter were obtained.

The effects of the different sintering parameters on the cathode surface morphology were investigated by SEM micrographs. As it was mentioned in Chapter 3, firstly all TCO glasses were sintered 5 minutes at 400 ^{o}C. Then, further annealing conditions given in Table 3.1 were applied. The resulting SEM micrographs at 50.000 magnification were given in Figure 4.1. It should be noted here that the SEM pictures do not distinguish Pt particles from that of SnO_2. Thus, the analysis provided below is for the whole surface.

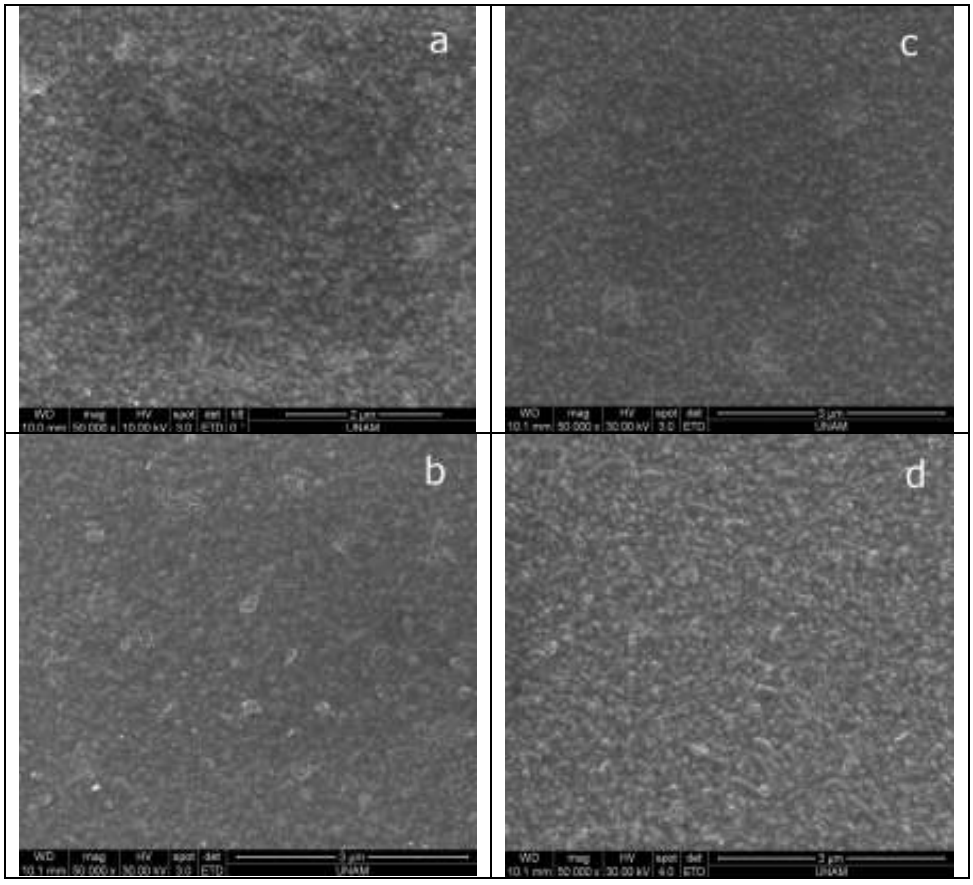

Figure 4.1. SEM micrographs at 50.000 magnification of (a) sample 1 (b) sample 2 (c) sample 3 (d) sample 4

SEM micrographs given in Figure 4.1 were used to perform an image analysis by the MedCalc Digimizer 3.7.0.0 software to see the changes in average particle length, perimeter and area of the surface. Also, the same software was used to prepare the data to perform particle area distribution analysis to see the effect of the annealing temperature to the particle size distributions. The results of the image analysis for the surface are summarized in Table 4.1.

Table 4.1 Image analysis results of the samples

Sample	**Parameter**	**Mean**	**Unit**
1	Average Area	0,007	μm^2
	Average Perimeter	354	nm
	Average Length	89	nm
2	Average Area	0,006	μm^2
	Average Perimeter	348	nm
	Average Length	83	nm
3	Average Area	0,005	μm^2
	Average Perimeter	268	nm
	Average Length	69	nm
4	Average Area	0,004	μm^2
	Average Perimeter	242	nm
	Average Length	67	nm

As it is seen in Table 4.1, as the sintering temperature increased, average particle length, perimeter and area of the surface decreased. Because area and perimeter are proportional to length, it was an

expected resulted for having similar results for length, area and perimeter with respect to sintering temperature.
However, the effect of temperature change on the change on particle sizes was not the same. For instance, although there was a large difference between the average particles sizes of sample 1 and sample 2, there was no such a difference between sample 3 and sample 4.

Particle area distributions given in Figure 4.2 to 4.5 confirmed that as the temperature increased, surface morphology changed because the peaks shifted left as the annealing temperature increased. It is emphasized that only the particles having the area of 0-0.08 μm^2 were shown in the particle distribution figures to show the peaks of the figures better. As it is seen in Figures 4.2 to 4.5, a second peak in the particle size distribution curve appeared as the annealing temperature increased. Also, no noticeable difference between Figure 4.4 and 4.5 can be observed.

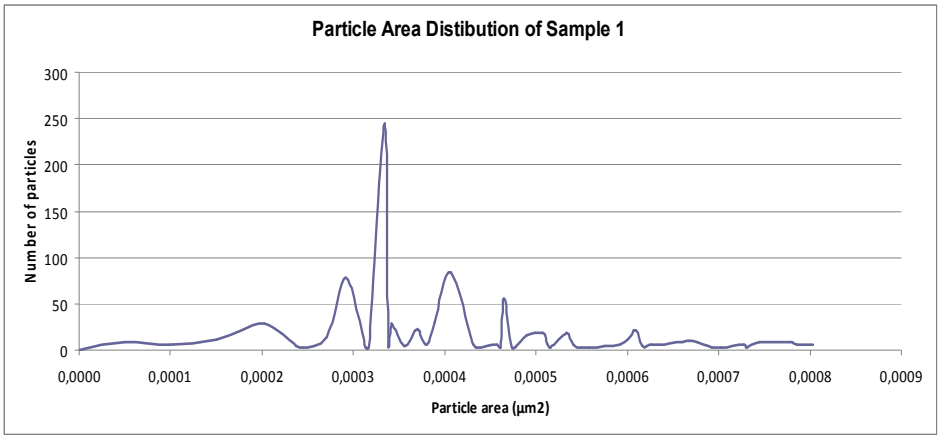

Figure 4.2. Particle area distribution of sample 1

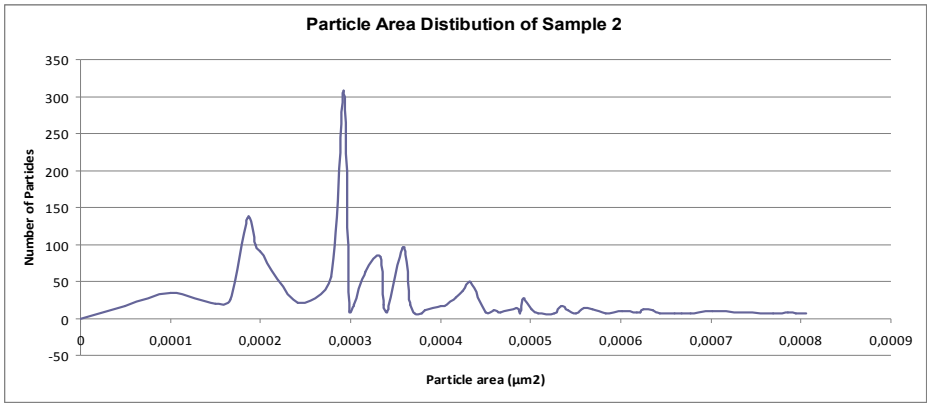

Figure 4.3. Particle area distribution of sample 2

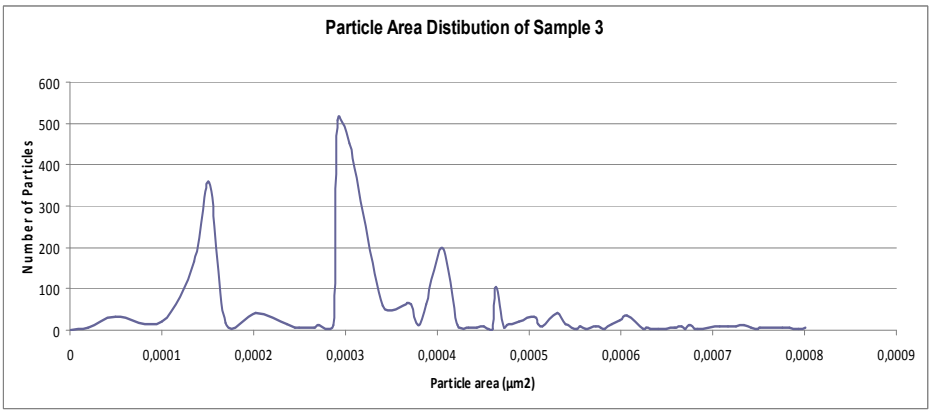

Figure 4.4. Particle area distribution of sample 3

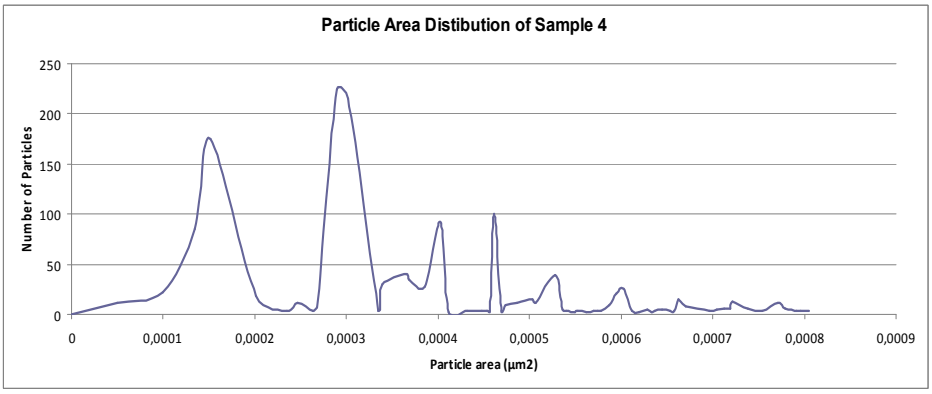

Figure 4.5. Particle area distribution of sample 4

In addition to the top view SEM micrographs, the side view of the sample 1 is given in Figure 4.6.

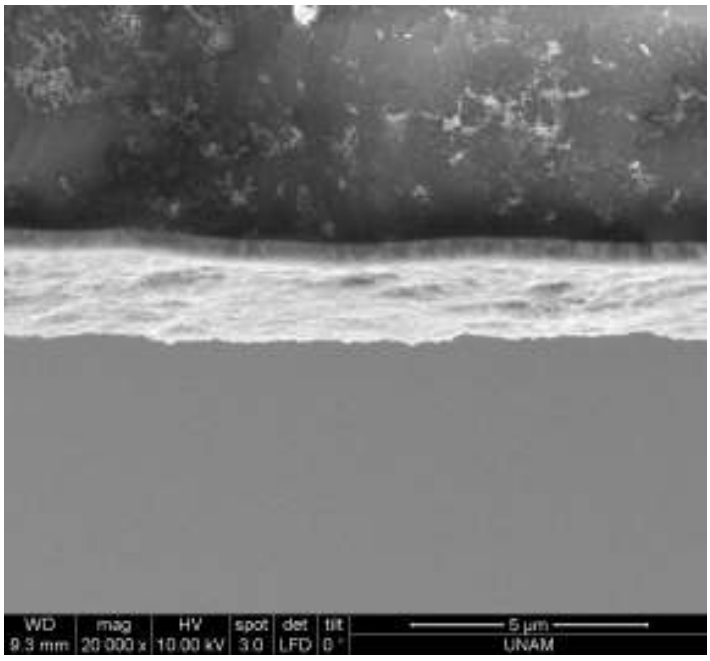

Figure 4.6. Side view of platinum covered TCO

It was hard to distinguish SnO_2 and Pt by using SEM micrographs as it is seen in Figure 4.6. Fang *et al*. [37] and Hauch and Georg [12] also agreed with the difficulty to determine the exact thickness by SEM micrographs and that was the reason why they could not determine the exact thickness of the platinum even though they were sure about that Pt thickness was at least 2 nm by thermal decomposition method.

Moreover, further SEM micrographs at much higher magnification were taken to see the morphological differences between different sintering conditions described in Table 3.1.

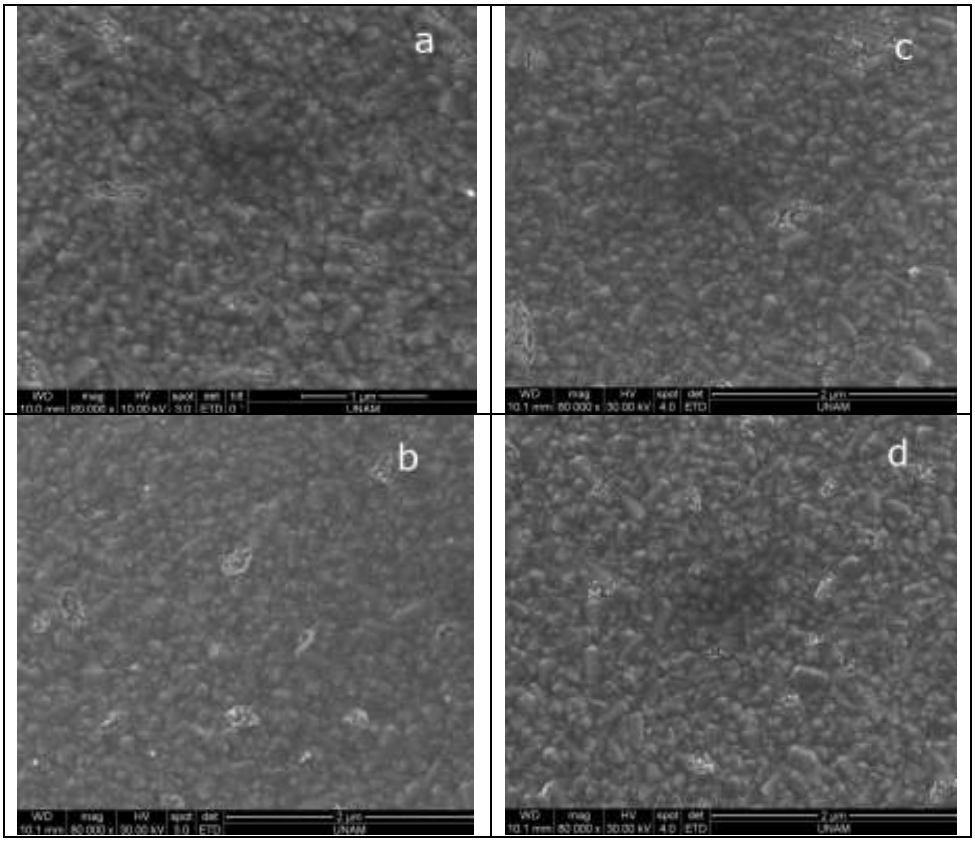

Figure 4.7. SEM micrographs at 80.000 magnification of (a) sample 1 (b) sample 2 (c) sample 3 (d) sample 4

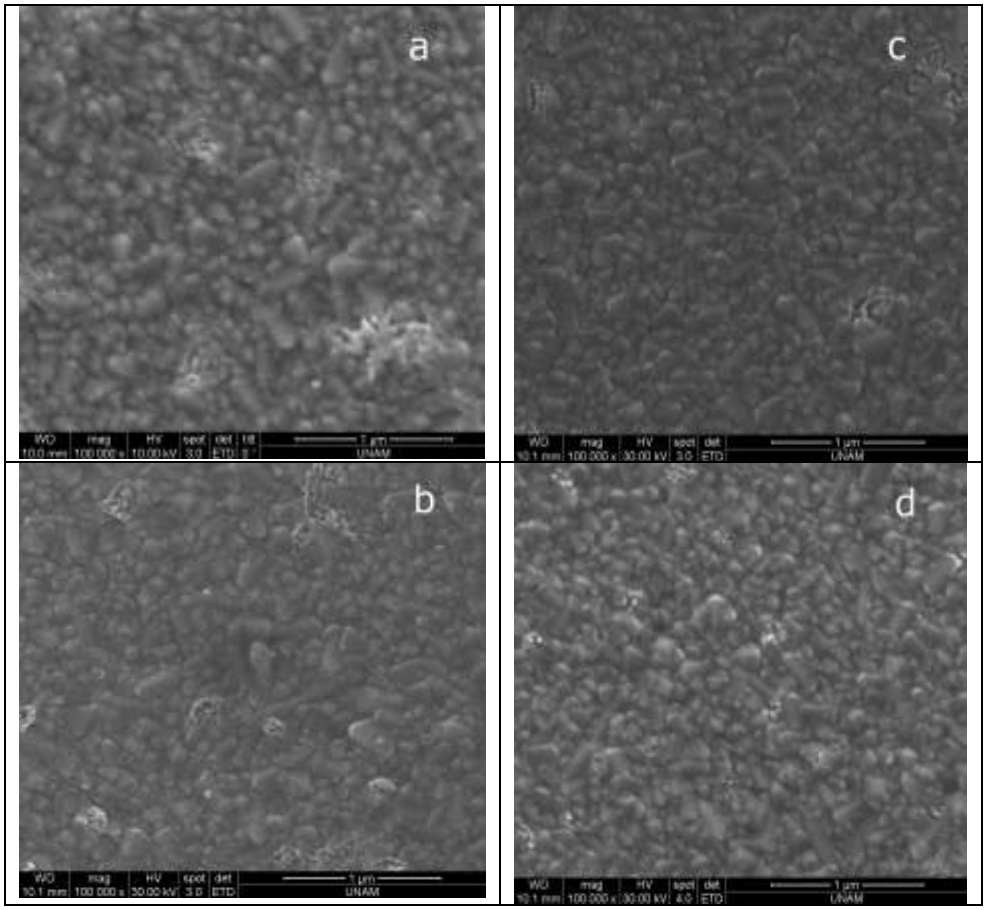

Figure 4.8. SEM micrographs at 100.000 magnification of (a) sample 1 (b) sample 2 (c) sample 3 (d) sample 4

According to Figure 4.7 and 4.8, it can easily be confirmed that particles get smaller as the sintering temperature gets higher which is in consistent with the results given in Table 4.1. Besides, decrease in roughness of the surface could be observed visually in Figure 4.7 and 4.8 due to decrease in particles sizes. Moreover, it is clearly seen that particle size of sample 1 is much higher than sample 4. However, there is no such noticeable difference between sample 3 and sample 4.

TEM micrographs are very critical to make further comments about the surface. However, TEM micrographs could not be taken because the TCO glasses taken from Solaronix are extra reinforced and they can not be thinned enough for TEM measurements. Thus, the literature micrographs are used for further comments. It is emphasized that thermal decomposition of platinum on SnO_2 coated glass were used both in this study and the studies whose TEM micrographs are given in Figure 4.9 to 4.11.

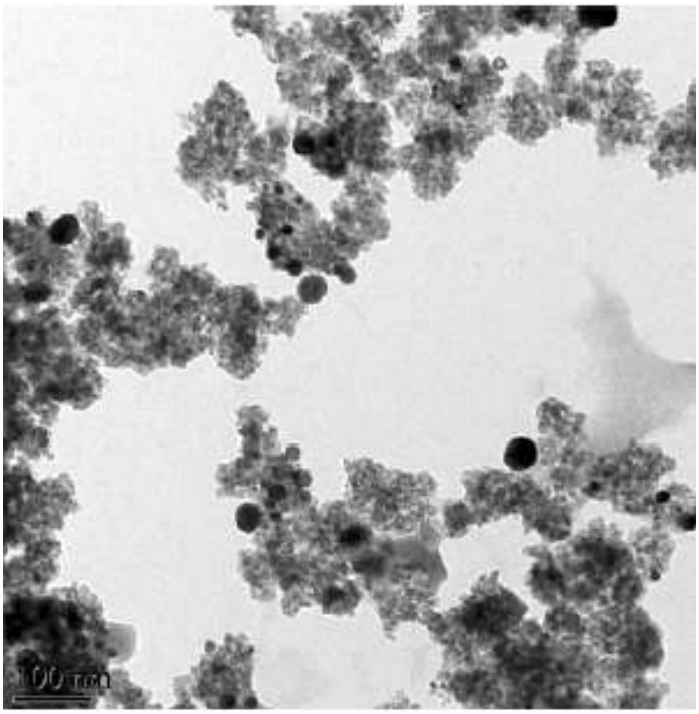

Figure 4.9. TEM image of the platinum nanoclusters on the TCO [32]

As it is seen in Figure 4.9, nano size platinum clusters are formed over the TCO. Besides, as the annealing temperature of thermal decomposition of platinum over TCO increased, nano clusters started to agglomerate according to Khelashvili *et al*. [33].

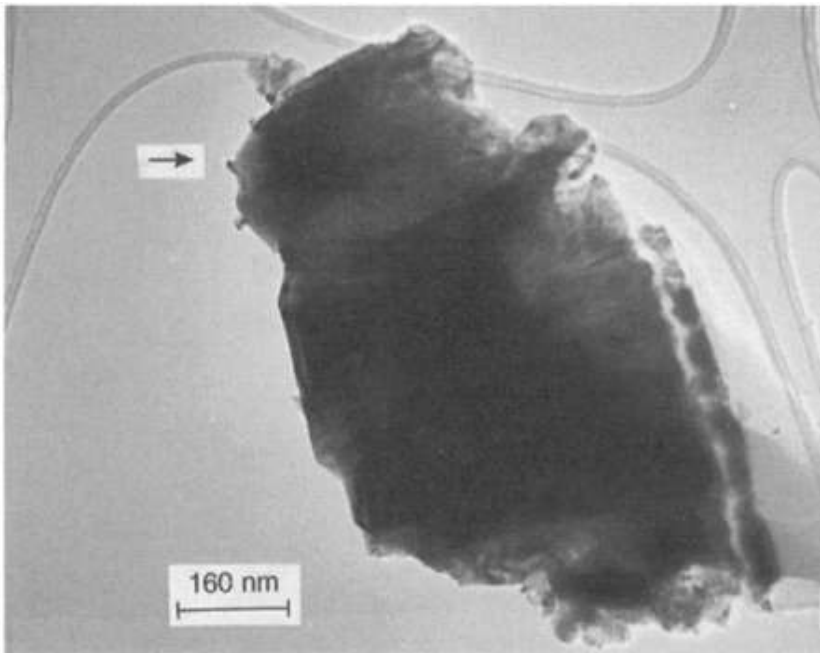

Figure 4.10. HRTEM of a platinized TCO [31]

The platinum nanocluster is shown by the arrow in Figure 4.10. As it is seen in the figure, nano cluster platinum is bound to SnO_2 on the glass. Since SEM pictures did not reveal clearly whether the morphology change was due to Pt or due to the substrate, backscattered electron analysis was performed to differentiate heavy Pt from much lighter Sn and Si present in the substrate.

In Figure 4.11 and 4.12, backscattered electron images of the counter electrode are shown. Figure 4.11 is the set of 100k magnified pictures taken from dense Pt regions while Figure 4.12 is the set of 80k magnification pictures taken from the regions where Pt coating was not dense.

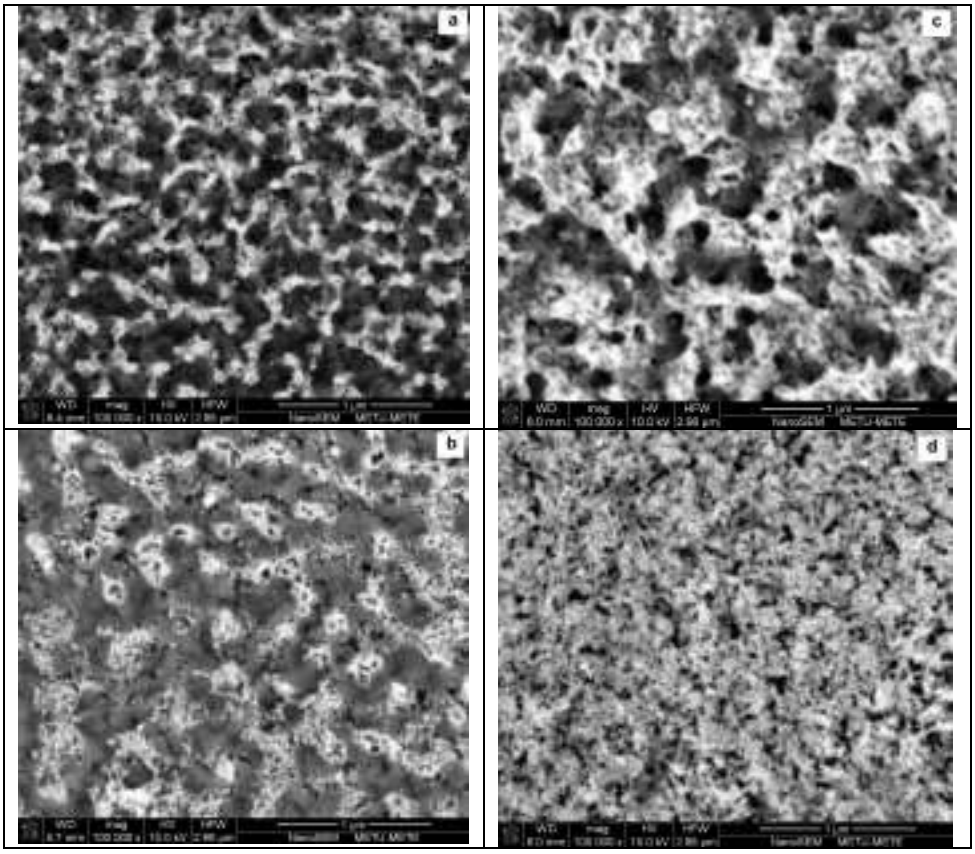

Figure 4.11. Figure 4.8. Backscattered electron images from Pt dense area at 100.000 magnification of (a) sample 1 (b) sample 2 (c) sample 3 (d) sample 4

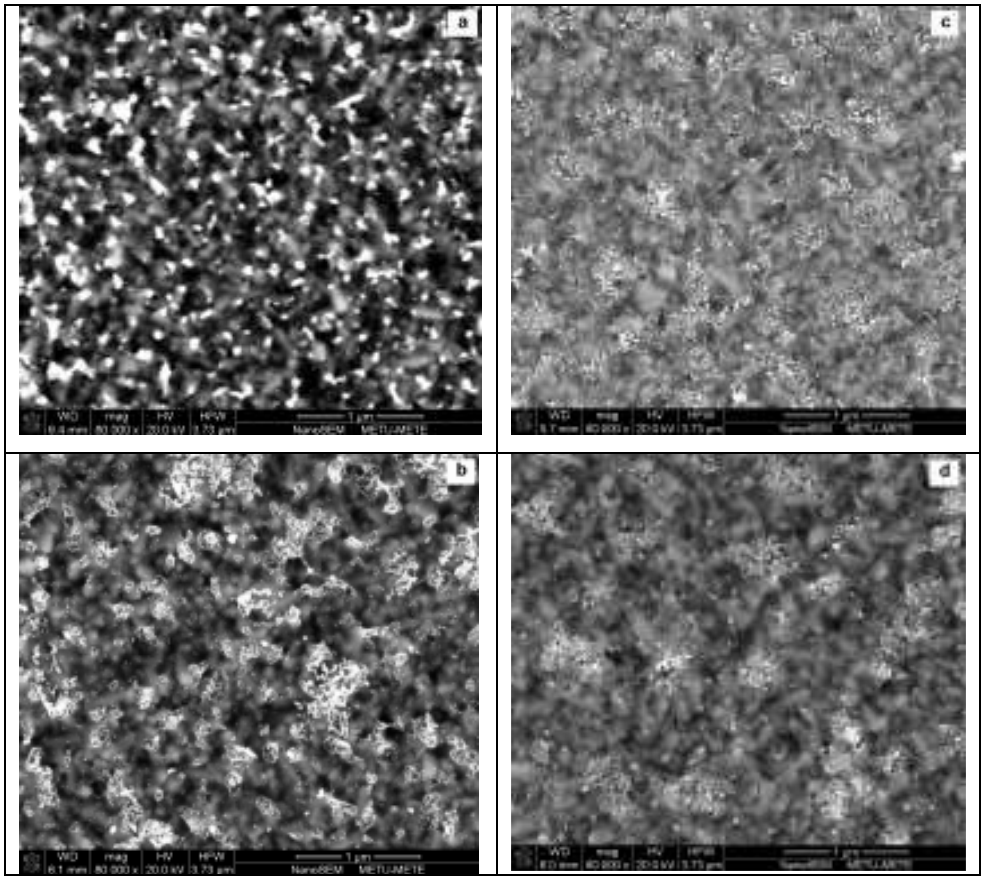

Figure 4.12. Backscattered electron images from Pt sparse area at 80.000 magnification of (a) sample 1 (b) sample 2 (c) sample 3 (d) sample 4

From the Figures 4.11 and 4.12, it was clearly seen that the Pt over layer structure has changed significantly with thermal annealing. As the annealing temperature increased, the dense regions grew denser and their structure changed. On the other hand, the regions where Pt was sparse, the amount of Pt decreased indicating that Pt has agglomerated into a film like structure with increasing annealing temperature. Moreover, In Figure 4.13 and 4.14, EDX of Sn and Pt maps are shown respectively which further supports the agglomeration hypothesis mentioned above.

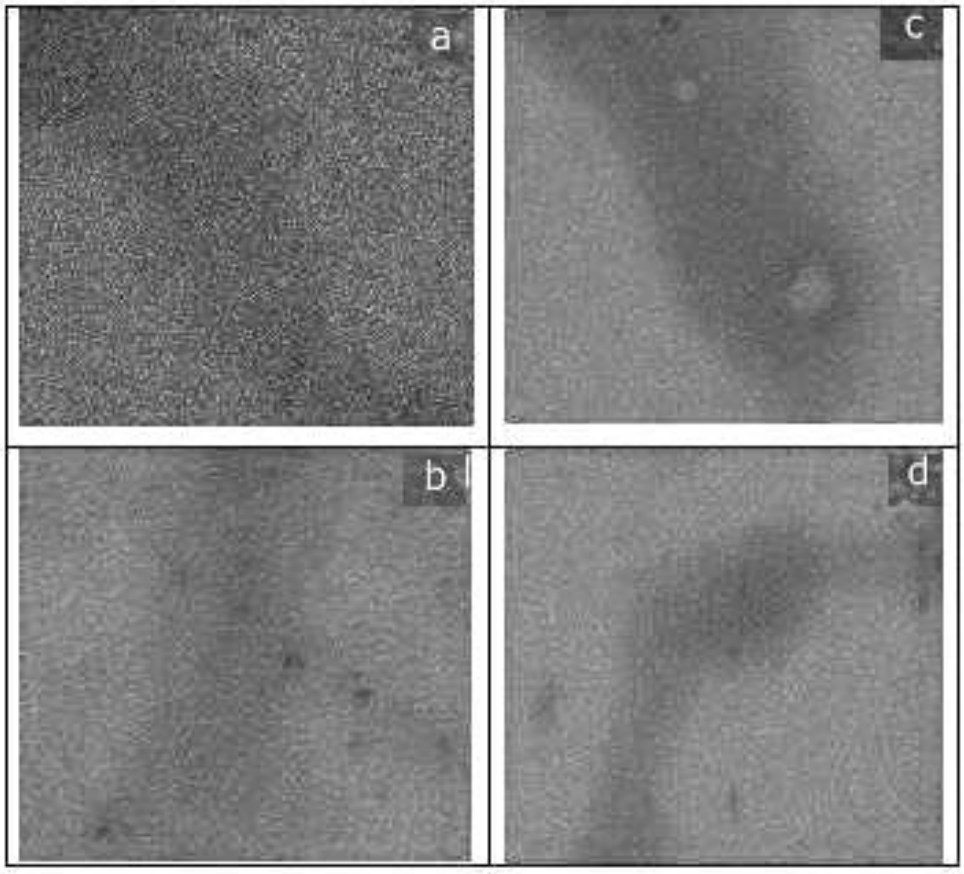

Figure 4.13. EDX mapping for Sn of (a) sample 1 (b) sample 2 (c) sample 3 (d) sample 4

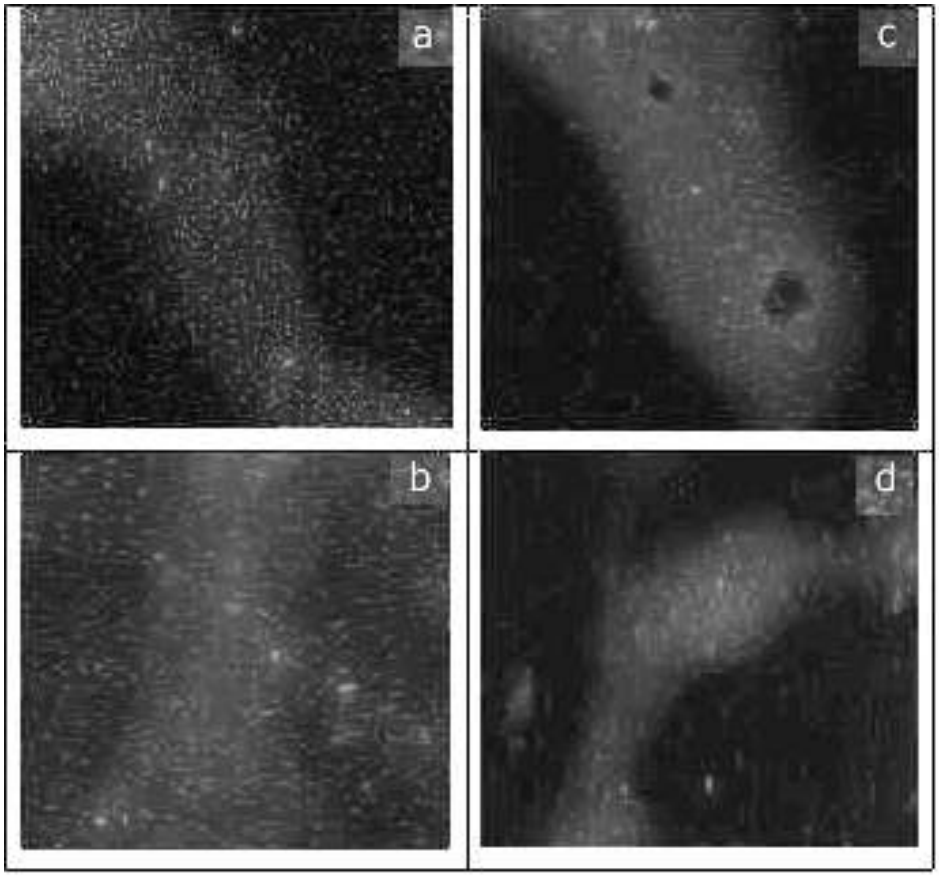

Figure 4.14. EDX mapping for Pt of (a) sample 1 (b) sample 2 (c) sample 3 (d) sample 4

Current and voltage values were measured as described in Chapter 3. The results are given in Figure 4.15 and the current-voltage values are also tabulated in Table A.2 - A.5 in Appendix A. The open circuit voltages and short circuit current densities are given in Table 4.2.

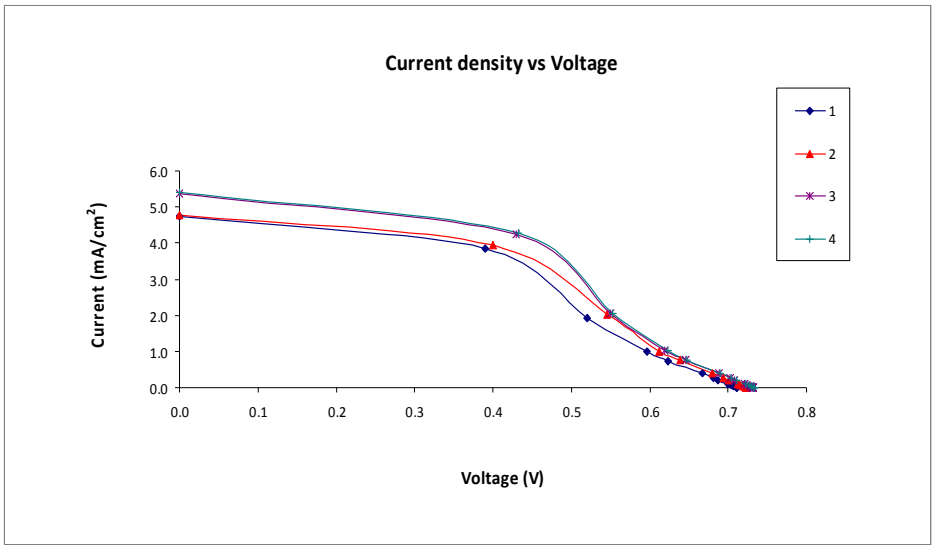

Figure 4.15. Current and voltage values of the samples under 650 W/m^2

Table 4.2. Open circuit voltage and short circuit current densities

Sample	V_{oc} (V)	j_{sc} (mA/cm^2)
1	0.712	4.74
2	0.724	4.78
3	0.732	5.36
4	0.735	5.39

As it clearly seen in both Figure 4.15 and Table 4.2, as the sintering temperature increases, current values and voltage values are increased. Also there was a noticeable improvement between sample 1 and sample 3, but no large difference existed between sample 3 and sample 4.

Power values were calculated as described in Chapter 3. Also a sample calculation is given Appendix B. The results are given in Figure 4.16 and power-voltage values are tabulated in Table A.6 in Appendix A.

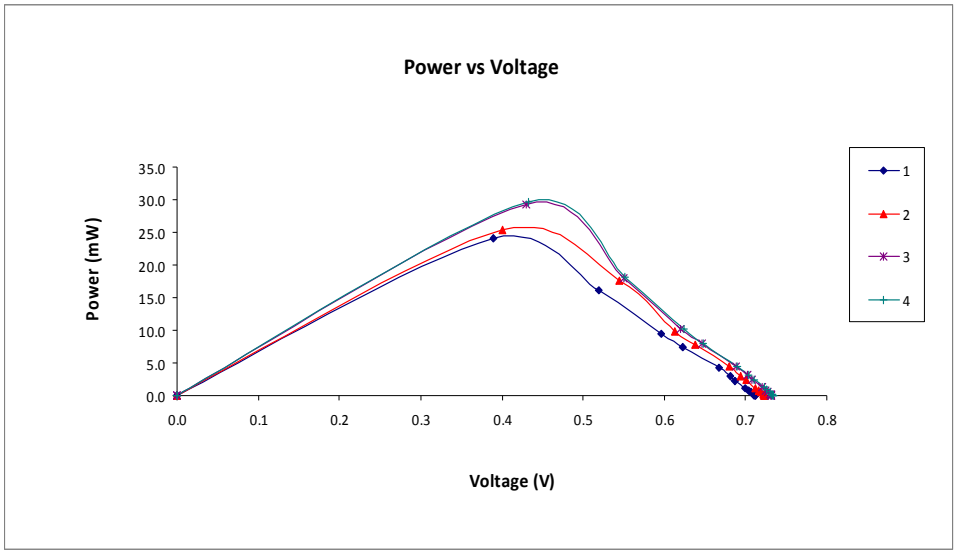

Figure 4.16. Power values according to measured voltages

The sequencing of power curves according to the voltages is the same with the sequencing of current values according to voltages. This is an expected result because power is directly proportional to current. Also there was a noticeable difference between sample 1 and sample 3, but no large difference existed between sample 3 and sample 4.

Power, filling factor and efficiencies are summarized in Table 4.3. A sample calculation is also given in Appendix B.

Table 4.3. Power, filling factor and efficiency of the samples

Sample	Substrate average particles size (nm)	Power (mW)	Filling factor	Efficiency (%)
1	89	24,50	0.454	2.36
2	83	25,80	0.466	2.48
3	69	29,60	0.471	2.85
4	67	30,00	0.474	2.89

Because the efficiency is directly proportional to current and voltage values, it was an expected result for having the highest efficiency from sample 4 which has the highest current and voltage values and it was an expected result for having the least efficiency form sample 1 which has the lowest current and voltage values. Because there is no significant increase from sample 3 to sample 4, sintering conditions for sample 3 can be recommended as the optimum one.

Also, it is known that filling factor describes the quality of the cell and it is related to efficiency [5]. The comments on the efficiencies are all valid for the filling factors. This is an expected result because as it is given in equation (1-5) and (1-8), their calculations are very similar mathematically.

In this study, it was found that as the annealing temperature of the counter electrode increased, performance parameters which are current-voltage, power-voltage and efficiency values increased too as it is clearly seen in Table 4.3. It was an expected result for having the same sequence of current, power and efficiency values according to

the annealing temperatures because power and efficiency values are directly proportional to current mathematically.

The first possible reason for the improvement in performance parameters could be the formation of film like coating of the platinum over the cathode surface. It was found in this study that the surface particle size was decreased by increasing the annealing temperature. Besides, it was also shown that Pt particles started to be agglomerated at higher annealing temperatures. Consequently, agglomeration of the platinum particles and decreasing the average particle sizes could result in forming a film like structure to cause an increase in performance parameters. Besides, it is emphasized that the sequence of performance parameters were the same with the sequence of average particle sizes. Moreover, this phenomenon can be the reason why the performance parameters of sample 3 and sample 4 are similar, whose average particles sizes were similar to each other.

The second possible reason for the increase in the performance parameters could be the change in oxidation state of platinum particles on the surface. It is known that zero valent state of platinum is better for the iodide/triiodide catalytic reaction and increasing the annealing temperature increases the percentage of zero valent state platinum particles according to both Bönnemann *et al*. [32] and Khelashvili *et al*. [33]. Thus, because Khelashvili *et al.* stated that all of the platinum oxidation states transformed to zero valent state at 580 ^{o} C, it was a reasonable result for having the largest efficiency from sample 4 which was annealed at 550 ^{o} C.

Besides, when a comparison is made for the performance parameters given in Table 1.2, it can be seen that efficiency of this

study is lower than the literature vales. The first possible reason why the current and efficiency of this study were lower than the efficiencies given in Table 1.2 is that some of TiO_2 particles may break off from anode side and adsorb on platinum. According to Hauch and Georg [12], weak adhesion may result in a back current in the cell which causes a major decrease in current and efficiency. Also another possible reason is the weak sealing of the DSSC. Weak sealing could cause an electrolyte loss by leaking from the edges of the DSSC which result in decreasing regeneration capacity of the DSSC.

Finally, an optimization suggestion can be made among the annealing conditions given in Table 3.1. Measured cell efficiency increased as the annealing temperature increased. However, because there is not a large difference between sample 3 and sample 4, it is suggested 30 minute at 500 ^{o}C after 5 minute at 400 ^{o} C annealing is the optimum condition.

CHAPTER 5

CONCLUSIONS

The aim of this study was to investigate the effects of the platinum particle sizes on the efficiency of a Dye Sensitized Solar Cell (DSCC).

It was shown that platinum was deposited as nano sized clusters by thermal decomposition method according to TEM micrographs. Moreover, according to the image analysis of the SEM micrographs, as the annealing temperature increased, average surface particle size decreased. It was also concluded that Pt particles started to agglomerate as the annealing temperature increased according to SEM micrographs and EDX mappings.

In this study, it was found that as the annealing temperature of cathode increased, efficiency increased also. Efficiency increased from 2.36% to 2.89 % and open circuit voltage and short circuit current density values are increased from 0.712 V and 4.74 mA/cm^2 to 0.735 V and 5.39 mA/cm^2 respectively by changing the platinization annealing and/or decomposition conditions from 5 minute at 400 ^{o} C to 30 minutes at 550 ^{o} C after 5 minute at 400 ^{o} C.

The increase in efficiency was attributed to two main reasons. Firstly, in this study, it was shown that as the annealing temperature of cathode side was increased, average surface particles size was

decreased. Decrease in average surface particle size could result that platinum clusters could form a film like coating over the surface. Moreover, it was shown that platinum cluster sizes increased at higher temperatures. Thus, larger cluster sizes could help to the formation of film like platinum coating over the surface to increase the efficiency. Secondly, as the temperature increases, oxidation state of the platinum changed such that percentage of zero valent state platinum increased. As it is known that zero valent state platinum shows a better catalytic activity for iodide/triiodide reaction, increasing the zero valent oxidation state platinum percentage could help increasing efficiency.

CHAPTER 6

RECOMMENDATIONS

In this study, the effects of the platinum particle sizes on the efficiency of a Dye Sensitized Solar Cell were investigated. Because a large effort was performed on preparing the cell first time in the laboratory, only most important and critical measurements and analysis could be made in remaining time schedule. Also, well known materials are used as components to focus on only the aim of the study. Thus, some recommendations can be made about further analysis and other materials for DSSC.

Firstly, nanotube TiO_2 structures are also promising materials for the anode side of the DSSC. A further research on the nanotube can be made to raise the efficiency. Also, new sensitizers especially the ones made in Turkey can be used to prepare the cell so if a domestic DSSC production start, an experience on a domestic sensitizer will be useful. Moreover, further assembly techniques can be studied to increase the cell life because leakage of the electrolyte will reduce the life of the cell considerably. Besides, alternative materials to platinum for the cathode side of the cell can be studied to reduce the DSSC cost.

Secondly, cyclic voltammetry measurements are recommended to understand the active surface areas of the cathode side. Also, further

TEM analysis can be performed to more understand behavior of the platinum crystal shapes under different annealing conditions.

REFERENCES

1. World Energy Council; *2004 Survey of Energy Resources,* Oxford, **2004**.
2. International Energy Agency; *Energy Policies of IEA Countries* Paris, **2005**.
3. Ministry of Energy and Natural Resources; *Workgroup Report for the Decreasing Greenhouse Gases in Energy Sector*, Ankara, **2005**.
4. Turkish Industrialist's and Businessmen's Association; *The Assessment of the Turkey's Energy Strategy at the Beginning of 21. Century,* İstanbul, **1998**.
5. Sterling, V.A. *Planning and installing photovoltaic systems: a guide for installers, architects, and engineers;* James & James / Earthscan, London, 2008.
6. O'Regan, B.; Gratzel, M. *Nature* **1991**, 353, 737-739.
7. Nazeeruddin, M. K.; De Angelis, F.; Fantacci, S.; Selloni, A.; Viscardi, G.; Liska, P.; Ito, S.; Bessho, T.; Gratzel, M. *Journal of American Chemical Society* **2005**, 127, 16835-16847.
8. Hagfeldt, A.; Gratzel, M. *Accounts of Chemical Research* **2000,** 33, 269-277.
9. Yoon, C.H.; Vittal, R.; Lee, J.; Chae, W.S.; Kim, K.J. Electrochimica Acta **2008**, 53, 2890-2896.
10. Smestad, G.; Bignozzi, C.; Argazzi R. *Solar Energy Materials and Solar Cells* **1994**, 32, 259-272.
11. Bolton, J. R.; Hall, D. O. *Photochemistry and Photobiology* **1991**, 53, 545.
12. Hauch, A.; Georg, A. *Electrochimica Acta* **2001**; 46; 3457-3466.

13. Nazeeruddin, M.K.; Kay, A.; Rodicio, I.; Baker, R.H.; Müller, E.; Liska, P.; Vlachopoulos, N.; Gratzel, M. *Journal of American Chemical Society* **1993**, 115, 6382-6390.

14. Gratzel, M. *Pure Applied Chemistry* **2001**, 73, 459–467.

15. Smestad, G.P. *Solar Energy Materials and Solar Cells* **1998**; 55; 157-178.

16. Tennakone, K.; Kumarasinghe, A.R., Kumara, G.R.R.A., Wijayantha, K.G.U.; Sirimanne, P. M. *Semiconductor Science Technology* **1995**; 10 ; 1689-1693.

17. Gratzel, M. *Journal of Photochemistry and Photobiology A: Chemistry* **2004**; 164; 3-14.

18. Kawano, R.; Matsui, H.; Matsuyama, C.; Sato, A.; Susan, M.A.B.H.; Tanabe, N., Watanabe, M. *Journal of Photochemistry and Photobiology A: Chemistry* **2004,** 164, , 87–92.

19. Barbe, C.J.; Arendse, F.; Comte, P.; Jirousek, M.; Lenzmann, F.; Shklover, V.; Gratzel, M. *Journal of the American Ceramic Society* **1997**, 80**,** 3157–3171.

20. Keis, K.; Vayssieres, L.; Lindquist, S.E.; Hagfeldt, A. *Nano Structured Materials* **1999**,12, 487-490.

21. Lee, S.H.A.; Abrams, N.M.; Hoertz, P.G.; Barber, G.D.; Halaoui, L.I.; Mallouk, T.E. The *Journal of Phyical Cheistry B* **2008**, 112 (46), 14415-14421.

22. Gomez, M.; Magnusson, E.; Olsson, E., Hagfeldt, A., Lindquist, S.E., Granqvist, C.G. *Solid State Physics* **1999**, 12, 146-149.

23. Nazeeruddin, M. K. ; Pechy, P. ; Gratzel, M. *Chemical Communications* **1997**, 18, 1705-1706.

24. Ela, S.E.; Yilmaz, M.D.; İcli, B.; Dede, Y.; İcli, S.; Akkaya, E.U. *Organic Letters* **2009**; 10 (15), 3299-3302.

25. Kay, A.; Gratzel, M. *Jornal of Phyical Chemistry* **1993**, *97*, 6272.

26. Kuang, D.; Walter, P.; Nuesch, F.; Kim, S.; Ko, J.; Comte, P.; Zakeeruddin, S.M.; Nazeeruddin, M.K.; Gratzel, M. *Langmuir* **2007,** *23,* 10906-10909.
27. Peter L.M.; Duffy N.W.; Wang R.L.; Wijayantha, K.G.U. Journal of Electroanalytical Chemistry **2002**, 524, 127-136.
28. Bay, L.; West, K.; Jensen, B.W.; Jacobsenn, T. *Solar Energy Materials & Solar Cells* **2006**; 90; 341–351.
29. Ikegami, M.; Miyoshi, K.; Miyasaka, T.; Wei, T. C.; Wan,C.C.; Wang, Y. Y. *Applied Physics Letters* **2007,** 153122, 90-92.
30. Kim, S.S.; Nah, Y.C.; Noh, Y.Y.; Jo, J.; Kim, D.Y. *Electrochimica Acta* **2006**, 51, 3814-3819.
31. Papageorgiou, N.; Maier, W.F.; Gratzel, M. *Journal of Electrochemical Society* **1997**, 144, 876-884.
32. Bönnemann, H.; Khelashvili, G.; Behrens, S.; Hinsch, A.; Skupien, K.; Dinjus E. *Journal of Cluster Science* **2006**, 18, 141-155.
33. Khelashvili, G.; Behrens, S.; Weidenthaler, C.; Vetter, C.; Hinsch, A; Kern, R.; Skupien, K.; Dinjus, E.; Bönnemann, H.; *Thin Solid Films* **2006**; 511- 512; 342- 348.
34. Kivrak, H.; Mastalir, A.; Kiraly, Z.; Uner, D. *Catalysis Communications* **2009** , 10, 1002-1005.
35. Uner, D.; Uner, M. *Thermochimica Acta* **2005**; 434; 107–112.
36. Solaronix, http://www.solaronix.com/products/platinumcatalysts/platisol/, last visited on 15.01.2010.
37. Fang, X.; Ma, T.; Guan, G.; Akiyama, M.; Kida, T.; Abe E. *Journal of Electroanalytical Chemistry* **2004**, 570, 257-263.
38. Amadelli, R.; Argazzi, R.; Bignozzi, C. A.; Scandola, F. *Jornal of American Chemical Society* **1990**, *112,* 7099-7103.

39. Anderson, C.; Bard, A.J. *Journal of Physical Chemistry* **1995**; 99; 9882-9885.

40. Bard, A.J.; Fox, M.A. *Accounts of Chemical Research* **1995**; 28; 141-145.

41. Boschloo, G.; Hagfeldt, A. *Accounts of Chemical Research* **2009**, *42,* 1819–1826.

42. Bredas, J.L.; Durrant, J.R.; *Accounts of Chemical Research* **2009**, *42*, 1689–1690.

43. Bredas, J.L.; Norton, J.E.; Cornil J.; Coropceanu, V. *Accounts of Chemical Research* **2009**, *42*, 1691–1699.

44. Chen, C.C.; Chung, H.W.; Chen, C.H.; Lu, H.P.; Lan, C.M.; Chen, S.F.; Luo, L.; Hung, C.S.; Diau, E.W.G. *Journal of Physical Chemistry C* **2008**, 112,19151–19157.

45. Chen, J.; Cao, Y. *Accounts of Chemical Research* **2009**, *42*, 709–1718

46. Cherepy, N.J.; Smestad, G.P.; Gratzel, M.; Zhang J.Z. *Journal of Physiscal Chemistry B* **1997**, *101,* 9342-9351.

47. Duncan, W.R.; Prezhdo, O.V. Annual Review of Physical Chemistry **2007**, 58, 143-184.

48. Villanueva, J.; Anta, J.A.; Guille, E.; Oksam, G. Journal *of Phyical. Chemistry C* **2009,** 113, 19722–19731.

49. Vlachopoulos, N.; Gratzel M. *Journal of the American Chemical Society* **1993,** *115,* 6382-6390.

50. Watson, D.F.; Meyer, G.J. *Annual Review of Physical Chemistry* **2005**, 56, 119-159.

51. Wei, T.C.; Wan, C.C.; Wang, Y.Y. *Applied Physics Letters* **2006**, 88, 103122-1-103122-3.

52. Yanagida, S.; Yu, Y.; Manseki, K. *Accounts of Chemical Research* **2009**, *42,* 1827–1838.

53. Zafer, C.; Karapire, C.; Sariciftci, N.S.; Icli, S. *Solar Energy Materials and Solar Cells* **2005**; 88; 11–21.
54. Zeet, J.; Heeger, A.J.; Bazen, G.C. *Accounts of Chemical Research* **2009**, *42,* 1700–1708.
55. Zweibel, K. *American Science* **1993**, 81, 362.
56. Heremans P.; Cheyns D.; Rand B.P. *Acconts of Chemical Research* **2009**, *42,* 1740–1747.
57. Inganas, O.; Zhang, F.; Andersson, M.R. *Accounts of Chemical Research* **2009**, *42,* 1731–1739
58. Ito, S.; Chen, P.; Comte, P.; Nazeeruddin, M.K.; Liska, P.; Pechy, P.; Gratzel M. *Progress in Photovoltaics* **2007**, 15, 603–612.
59. *Journal of Physical Chemistry B* **1997**, *101,* 2514-2518.
60. Papageorgiou, N. *Coordination Chemistry Reviews* **2004,** 248, 1421-1446.
61. Paulsson, H.; Kloo, L.; Hagfeldt, A.; Boschloo G. *Journal of Electroanalytical Chemistry* **2006**, 586, 56–61.

APPENDIX A

ELECTRICAL MEASUREMENTS

Table A.1. Resistances used during measurements

Number	R (kΩ)	Number	R (kΩ)
1	0.006	9	0.632
2	0.017	10	1.053
3	0.038	11	2.105
4	0.053	12	4.632
5	0.105	13	6.737
6	0.158	14	11.368
7	0.211	15	16.000
8	0.421		

Table A.2. Current-voltage measurements for the sample 1

V (V)	R (k Ω)	i (mA)	j (mA/cm^2)
0.390	0.006	61.750	3.859
0.520	0.017	30.875	1.930
0.597	0.038	15.749	0.984
0.623	0.053	11.841	0.740
0.667	0.105	6.337	0.396
0.681	0.158	4.313	0.270
0.688	0.211	3.266	0.204
0.699	0.421	1.661	0.104
0.703	0.632	1.114	0.070
0.707	1.053	0.671	0.042
0.709	2.105	0.337	0.021
0.711	4.632	0.153	0.010
0.711	6.737	0.106	0.007
0.711	11.368	0.063	0.004
0.712	16.000	0.044	0.003

Table A.3. Current-voltage measurements for the sample 2

V (V)	R (k Ω)	i (mA)	j (mA/cm^2)
0.400	0.006	63.333	3.958
0.545	0.017	32.359	2.022
0.613	0.038	16.163	1.010
0.638	0.053	12.130	0.758
0.680	0.105	6.460	0.404
0.693	0.158	4.392	0.274
0.701	0.211	3.329	0.208
0.712	0.421	1.691	0.106
0.716	0.632	1.134	0.071
0.719	1.053	0.683	0.043
0.721	2.105	0.343	0.021
0.723	4.632	0.156	0.010
0.723	6.737	0.107	0.007
0.723	11.368	0.064	0.004
0.724	16.000	0.045	0.003

Table A.4. Current-voltage measurements for the sample 3

V (V)	R (k Ω)	i (mA)	j (mA/cm^2)
0.430	0.006	68.083	4.255
0.550	0.017	32.656	2.041
0.620	0.038	16.353	1.022
0.646	0.053	12.282	0.768
0.689	0.105	6.543	0.409
0.703	0.158	4.449	0.278
0.708	0.211	3.365	0.210
0.721	0.421	1.711	0.107
0.724	0.632	1.146	0.072
0.728	1.053	0.691	0.043
0.730	2.105	0.347	0.022
0.731	4.632	0.158	0.010
0.731	6.737	0.109	0.007
0.732	11.368	0.064	0.004
0.732	16.000	0.046	0.003

Table A.5. Current-voltage measurements for the sample 4

V (V)	R (k Ω)	i (mA)	j (mA/cm^2)
0.433	0.006	68.558	4.285
0.552	0.017	32.775	2.048
0.624	0.038	16.453	1.028
0.648	0.053	12.306	0.769
0.690	0.105	6.557	0.410
0.704	0.158	4.456	0.278
0.711	0.211	3.375	0.211
0.723	0.421	1.716	0.107
0.727	0.632	1.150	0.072
0.730	1.053	0.693	0.043
0.731	2.105	0.347	0.022
0.733	4.632	0.158	0.010
0.734	6.737	0.109	0.007
0.734	11.368	0.065	0.004
0.734	16.000	0.046	0.003

Table A.6. Power (mW) values

Sample 1	Sample 2	Sample 3	Sample 4
24.083	25.333	29.276	29.686
16.055	17.636	17.961	18.092
9.399	9.900	10.134	10.259
7.379	7.744	7.939	7.971
4.228	4.393	4.506	4.526
2.937	3.045	3.126	3.134
2.245	2.333	2.384	2.399
1.162	1.204	1.233	1.240
0.783	0.811	0.830	0.836
0.474	0.491	0.503	0.506
0.239	0.247	0.253	0.254
0.109	0.113	0.115	0.116
0.075	0.078	0.079	0.080
0.045	0.046	0.047	0.047
0.032	0.033	0.033	0.034

APPENDIX B

SAMPLE PERFORMANCE PARAMETERS CALCULATIONS

The sample calculation for the sample 1 which was sintered at 400 ^{o}C for 5 minutes are given below. The measurement setup, characterization methods were given in Chapter 3.

Firstly, the voltage values are measured according to resistances under 650 W/m^2 light intensity. The results are summarized in Table A.1.

Secondly, the corresponding currents are calculated by using equation (1-6). Active area which is 16 cm^2 is used for finding current per area. Results are given in Table B.1.

Table B.1. Calculated current values for sample 1

V (V)	R (k Ω)	i (mA)	j (mA/cm^2)
0.390	0.006	61.750	3.859
0.520	0.017	30.875	1.930
0.597	0.038	15.749	0.984
0.623	0.053	11.841	0.740
0.667	0.105	6.337	0.396
0.681	0.158	4.313	0.270
0.688	0.211	3.266	0.204
0.699	0.421	1.661	0.104
0.703	0.632	1.114	0.070
0.707	1.053	0.671	0.042
0.709	2.105	0.337	0.021
0.711	4.632	0.153	0.010
0.711	6.737	0.106	0.007
0.711	11.368	0.063	0.004
0.712	16.000	0.044	0.003

It is emphasized that the V_{oc} is the x intercept and I_{sc} is the y intercept values in the current-voltage figures. The third step of the calculation is calculating power values corresponding to voltages.

Power values are calculated by equation (1-7) and given in Table A.6.

Fourth step is finding P_{MPP} which is the peak point of Power-voltage curve whose values are found in second step of calculation process. P_{MPP} is shown in Figure B.1.

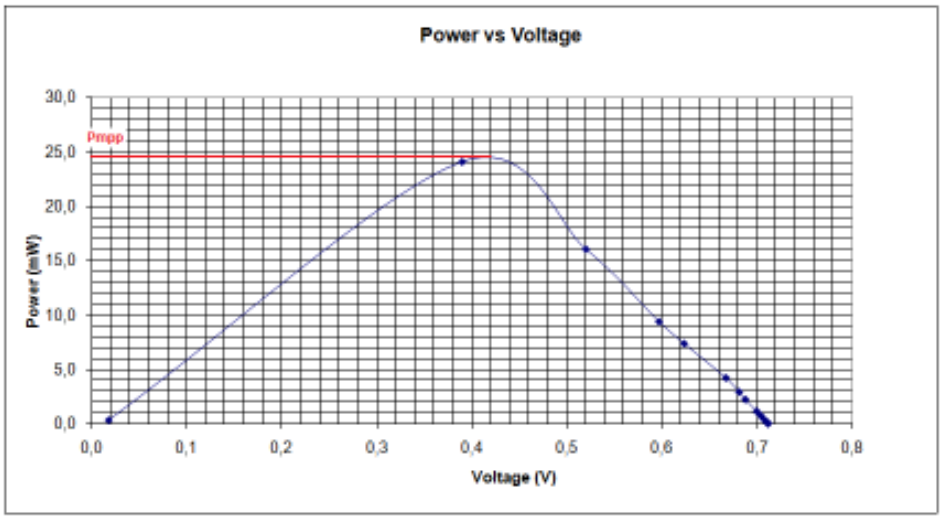

Figure B.1. Power-voltage curve for sample 1

Fifth step is finding efficiency of the DSSC. Recall equation (1-8).

$\eta = (P_{MPP}) / (AxE)$

$E = 650\ W/m^2$

$A = 16\ cm^2$

$P_{MPP} = 24.5\ mW$

Thus. efficiency is found as following:

$\eta = 24.5\ mW / [****(650\ W/m^2)x(0.0001\ cm^2/m^2)x16\ cm^2] *100$

= 2.356%

Final step is finding filling factor. Recall equation (1-5).

FF = P_{MPP} / Voc x Isc

V_{oc} = 0.712 V

I_{sc} = 75.840 mA

Thus, FF is found as following:

FF= 24.5 mW /(0.712 V * 75.840 mA) = 0.454

APPENDIX C

CURRENT - VOLTAGE MEASUREMENT SETUP

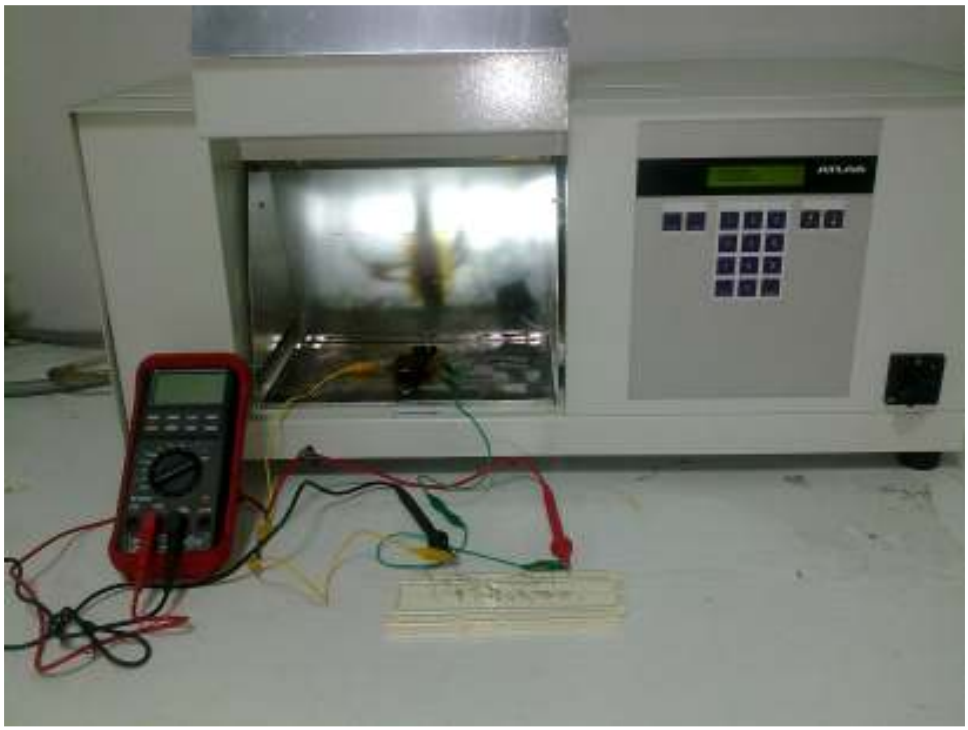

Figure C.1. Current-voltage measurement setup.